

000 AP-OOD: ATTENTION POOLING FOR OUT-OF- 001 002 DISTRIBUTION DETECTION 003 004

005 **Anonymous authors**

006 Paper under double-blind review

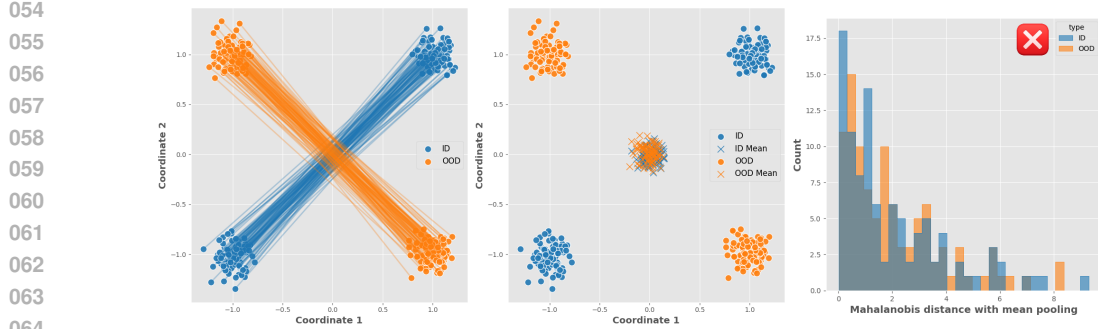
009 ABSTRACT 010

011 Out-of-distribution (OOD) detection, which maps high-dimensional data into
012 a scalar OOD score, is critical for the reliable deployment of machine learning
013 models. A key challenge in recent research is how to effectively leverage
014 and aggregate token embeddings from language models to obtain the OOD
015 score. In this work, we propose AP-OOD, a novel OOD detection method
016 for natural language that goes beyond simple average-based aggregation by
017 exploiting token-level information. AP-OOD is a semi-supervised approach
018 that flexibly interpolates between unsupervised and supervised settings,
019 enabling the use of limited auxiliary outlier data. Empirically, AP-OOD
020 sets a new state of the art in OOD detection for text: in the unsupervised
021 setting, it reduces the FPR95 (false positive rate at 95% true positives) from
022 27.77% to 5.91% on XSUM summarization, and from 75.19% to 68.13% on
023 WMT15 En–Fr translation.

024 1 INTRODUCTION 025

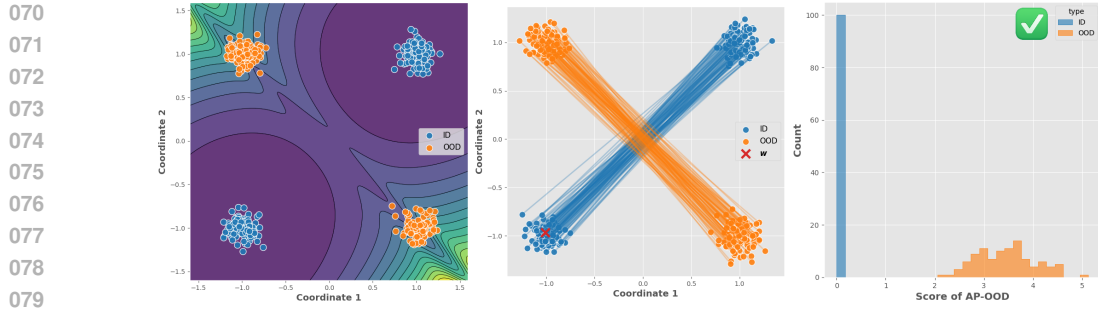
026 Out-of-distribution (OOD) detection is essential for deploying machine learning models in
027 the real world. In practical settings many models encounter inputs that deviate from the
028 model’s training distribution. For example, a model trained to summarize news articles
029 might also receive a prompt with a cooking recipe. In such situations, models may assign
030 unwarranted confidence to their predictions, leading to erroneous outputs **and hallucination**.
031 **A hallucination is a state in which the model generates output that is nonsensical or**
032 **unfaithful to the prompt** (Farquhar et al., 2024). For example, Ren et al. (2023) observe that
033 a common failure case in abstractive summarization is for the model to output “All images
034 are copyrighted” when prompted to summarize news articles from a publisher (CNN) that
035 differs from what it was trained on (BBC). Many authors attribute hallucination to model
036 uncertainty (e.g., Farquhar et al., 2024; Aichberger et al., 2025), which decomposes into
037 aleatoric uncertainty (resulting from noise in the data) and epistemic uncertainty (resulting
038 from a lack of training data). OOD prompts exhibit high epistemic uncertainty (Ren et al.,
039 2023). The purpose of OOD detection is to classify these inputs as OOD such that the
040 system can then, for instance, notify the user that no output can be generated. Many
041 existing post-hoc OOD detection methods (e.g., Huang et al., 2021; Sun & Li, 2022; Wang
042 et al., 2022) assume a classifier as the base model. In contrast, in language modeling, the
043 base model is typically an autoregressive generative model without an explicit classification
044 head. This necessitates the development of OOD detection methods specifically tailored for
045 language modeling, and we believe that the OOD detection community can benefit from
046 generative language modeling as an additional benchmark. Our contributions are as follows:

- 047 1. We propose AP-OOD, an OOD detection approach for natural language that leverages
048 token-level information to detect OOD sequences.
- 049 2. AP-OOD is a semi-supervised approach: It can be applied in unsupervised (i.e.,
050 when there exists no knowledge about OOD samples) and supervised settings (i.e.,
051 when some OOD data of interest is available to the practitioner), and smoothly
052 interpolates between the two.
- 053 3. We show that AP-OOD can improve OOD detection for natural language in summa-
054 rization and translation.



065
066
067
068
069

Figure 1: Illustrative example for the failure of mean pooling. **(Left)** ID and OOD sequences $Z_i \in \mathbb{R}^{2 \times 2}$, where each sequence contains a pair of token embeddings with two features each. Token embeddings that belong to the same sequence are connected with lines. **(Center)** The means of the ID and OOD sequences both cluster around the origin. **(Right)** A mean pooling approach cannot discriminate between the ID and OOD sequences.



080
081
082
083
084
085

Figure 2: Illustrative example for the mechanism that AP-OOD uses to correctly discriminate between ID and OOD (as opposed to the mean pooling approaches). The setting is the same as in Figure 1. **(Left)** The loss landscape forms two basins at the locations of the ID token embeddings. **(Center)** After training AP-OOD with a single weight vector w , the learned w is located in one of the basins. **(Right)** AP-OOD achieves perfect discrimination between the ID and OOD sequences.

086
087
088
089

4. We provide a theoretical motivation for the suitability of AP-OOD for OOD detection on tokenized data.

090
091

1.1 BACKGROUND

092
093
094
095
096

Consider a language model trained that given input sequences $(\mathbf{x}_1, \mathbf{x}_2, \dots, \mathbf{x}_N)$ with $\mathbf{x}_i \in \mathcal{X}^1$ autoregressively generates target sequences $(\mathbf{y}_1, \mathbf{y}_2, \dots, \mathbf{y}_N)$ with $\mathbf{y}_i \in \mathcal{X}$. The input sequences are drawn i.i.d.: $\mathbf{x}_i \sim p_{\text{ID}}$. We consider input sequences $\mathbf{x} \in \mathcal{X}$ that deviate considerably from the data generation $p_{\text{ID}}(\mathbf{x})$ that defines the “normality” of our data as OOD. Following Ruff et al. (2021), an observed sequence is OOD if it is an element of the set

$$\mathbb{O} := \{\mathbf{x} \in \mathcal{X} \mid p_{\text{ID}}(\mathbf{x}) < \epsilon\} \text{ where } \epsilon \geq 0, \quad (1)$$

097
098
099
100
101
102

and $\epsilon \in \mathbb{R}$ is a density threshold. In practice, it is common (e.g., Hendrycks & Gimpel, 2016; Lee et al., 2018; Hofmann et al., 2024) to define a score $s : \mathcal{Z} \rightarrow \mathbb{R}$ that uses an encoder $\phi : \mathcal{X} \rightarrow \mathcal{Z}$ (where \mathcal{Z} denotes an embedding space). Given s and ϕ , OOD detection can be formulated as a binary classification task with the classes in-distribution (ID) and OOD:

$$\hat{B}(\mathbf{x}, \gamma) = \begin{cases} \text{ID} & \text{if } s(\phi(\mathbf{x})) \geq \gamma \\ \text{OOD} & \text{if } s(\phi(\mathbf{x})) < \gamma \end{cases}. \quad (2)$$

103
104
105
106
107

The outlier score should — in the best case — preserve the density ranking, but it does not have to fulfill all requirements of a probability density (proper normalization or nonnegativity).

¹We use $\mathcal{X} := \bigcup_{S \geq 1} \mathcal{V}^S$ for the set of input sequences, and $\mathcal{V} := \{v_1, \dots, v_V\}$ is the vocabulary.

108 For evaluation, the threshold $\gamma \in \mathbb{R}$ is typically chosen such that 95% of ID samples from a
 109 previously unseen validation set are correctly classified as ID. However, metrics like the area
 110 under the receiver operating characteristic (AUROC) can be directly computed on $s(\phi(\mathbf{x}))$
 111 without fixing γ , since the AUROC sweeps over all possible thresholds.
 112

113 2 METHOD

116 AP-OOD is a semi-supervised method: It can be trained without access to outlier data
 117 (unsupervised), and with access to outlier data (supervised), and can smoothly transition
 118 between those two scenarios as more outlier data becomes available for training. In the
 119 following, we first introduce AP-OOD in an unsupervised scenario (Section 2.1) and generalize
 120 it to the supervised scenario (Section 2.2).
 121

122 2.1 UNSUPERVISED OOD DETECTION

123 **Background** Ren et al. (2023) propose to detect OOD inputs using token embeddings
 124 obtained from a transformer encoder–decoder model (Vaswani et al., 2017b) trained on
 125 the language modeling task. Given an input sequence \mathbf{x} , they obtain a sequence of token
 126 embeddings. They compare obtaining embeddings $\mathbf{E} \in \mathcal{Z}^2$ from the encoder $\phi_{\text{enc}} : \mathcal{X} \rightarrow \mathcal{Z}$
 127 and generating a sequence of embeddings $\mathbf{G} \in \mathcal{Z}$ using the decoder $\phi_{\text{dec}} : \mathcal{Z} \rightarrow \mathcal{Z}$:
 128

$$129 \quad \mathbf{E} := \phi_{\text{enc}}(\mathbf{x}) \quad \mathbf{G} := \phi_{\text{dec}}(\mathbf{E}). \quad (3)$$

130 For clarity, we write $\mathbf{Z} \in \mathcal{Z}$ for a sequence of token embeddings, whether produced by the
 131 encoder or the decoder, and we call \mathbf{Z} the sequence representation of \mathbf{x} . To obtain a single
 132 vector $\bar{\mathbf{z}} \in \mathbb{R}^D$, Ren et al. (2023) perform mean pooling:
 133

$$134 \quad \bar{\mathbf{z}} := \frac{1}{S} \sum_{s=1}^S \mathbf{z}_s. \quad (4)$$

135 Then, they propose to measure whether $\bar{\mathbf{z}}$ is OOD by first fitting a Gaussian distribution
 136 $\mathcal{N}(\boldsymbol{\mu}, \boldsymbol{\Sigma})$, $\boldsymbol{\mu} \in \mathbb{R}^D$, $\boldsymbol{\Sigma} \in \mathbb{R}^{D \times D}$ to the per-sequence mean embeddings computed from the
 137 training corpus, and then computing the squared Mahalanobis distance between $\bar{\mathbf{z}}$ and $\boldsymbol{\mu}$:
 138

$$141 \quad d_{\text{Maha}}^2(\bar{\mathbf{z}}, \boldsymbol{\mu}) := (\bar{\mathbf{z}} - \boldsymbol{\mu})^T \boldsymbol{\Sigma}^{-1} (\bar{\mathbf{z}} - \boldsymbol{\mu}) \quad \text{and} \quad s_{\text{Maha}}(\bar{\mathbf{z}}) := -d_{\text{Maha}}^2(\bar{\mathbf{z}}, \boldsymbol{\mu}). \quad (5)$$

143 **Averaging hides anomalies.** The key limitation of the approach described above is the
 144 use of the **mean** of the token embeddings \mathbf{Z} : Averaging the entire sequence into the mean $\bar{\mathbf{z}}$
 145 discards the token-level structure that would otherwise be informative for detecting whether
 146 a sequence is OOD. Figure 1 shows a toy example of this failure mode: The ID and OOD
 147 sequences are indistinguishable using their means, and therefore, the Mahalanobis distance
 148 with mean pooling fails to discriminate between them.
 149

150 **Mahalanobis decomposition.** To address this limitation, we begin by expressing the
 151 Mahalanobis distance as a directional decomposition:
 152

$$153 \quad d_{\text{Maha}}^2(\bar{\mathbf{z}}, \boldsymbol{\mu}) = \sum_{j=1}^D (\mathbf{w}_j^T \bar{\mathbf{z}} - \mathbf{w}_j^T \boldsymbol{\mu})^2, \quad (6)$$

156 The weight vectors $\mathbf{w}_j \in \mathbb{R}^D$ form a basis of \mathbb{R}^D and determine $\boldsymbol{\Sigma}^{-1}$ via $\boldsymbol{\Sigma}^{-1} = \sum_{j=1}^D \mathbf{w}_j \mathbf{w}_j^T$.
 157 One possibility to map a given $\boldsymbol{\Sigma}^{-1}$ to weight vectors \mathbf{w}_j is to select the directions of the
 158 \mathbf{w}_j as the unit-norm eigenvectors of $\boldsymbol{\Sigma}^{-1}$, and to select the squared norms of the \mathbf{w}_j as their
 159 corresponding eigenvalues (see Appendix B.2).
 160

161 ²We use $\mathcal{Z} := \bigcup_{S \geq 1} \mathbb{R}^{D \times S}$ for all finite-length sequences of D -dimensional token embeddings.

Algorithm 1 AP-OOD

```

162
163 Require:  $(\mathbf{x}_1, \dots, \mathbf{x}_N)$ ,  $\phi_{\text{enc}}$ ,  $\phi_{\text{dec}}$ ,  $\beta$ ,  $M$ , nsteps
164 1: for  $i = 1$  to  $N$  do
165 2:   Compute sequence embedding  $\mathbf{Z}_i \leftarrow \phi_{\text{enc}}(\mathbf{x}_i)$  or  $\mathbf{Z}_i \leftarrow \phi_{\text{dec}}(\phi_{\text{enc}}(\mathbf{x}_i))$ .
166 3: for step = 1 to nsteps do
167 4:   Randomly sample mini-batch indices  $\mathcal{B} \subset \{1, \dots, N\}$ 
168 5:   Collect mini-batch  $\{\mathbf{Z}_i\}_{i \in \mathcal{B}}$ .
169 6:   Form batch-local concatenation  $\tilde{\mathbf{Z}}_B \leftarrow \parallel_{i \in \mathcal{B}} \mathbf{Z}_i$ .
170 7:   Compute loss  $\mathcal{L} \leftarrow \frac{1}{|\mathcal{B}|} \sum_{i \in \mathcal{B}} d^2(\mathbf{Z}_i, \tilde{\mathbf{Z}}_B) - \sum_{j=1}^M \log(\|\mathbf{w}_j\|_2^2)$ .
171 8:   Compute gradients of  $\mathcal{L}$  w.r.t.  $(\mathbf{w}_1, \dots, \mathbf{w}_M)$  and perform a gradient update
172 9:   Do mini-batch attention pooling to compute  $\boldsymbol{\mu}_j \leftarrow \tilde{\mathbf{Z}} \text{softmax}(\beta \tilde{\mathbf{Z}}^T \mathbf{w}_j)$  (Appendix C.1)
173 10:   $s(\mathbf{Z}) \leftarrow \sum_{j=1}^M -d_j^2(\mathbf{Z}, \tilde{\mathbf{Z}}) + \log(\|\mathbf{w}_j\|_2^2)$ .
174 11: return  $s(\cdot)$ 
175
176
177

```

Beyond mean pooling. To overcome the limitations of mean pooling, we generalize Equation (6) by using attention pooling (Bahdanau, 2014; Ramsauer et al., 2021):

$$\text{AttPool}_\beta(\mathbf{Z}, \mathbf{w}) := \mathbf{Z} \text{softmax}(\beta \mathbf{Z}^T \mathbf{w}) \quad \text{and} \quad \bar{\mathbf{z}} := \text{AttPool}_\beta(\mathbf{Z}, \mathbf{w}). \quad (7)$$

where $\beta \in \mathbb{R}_{\geq 0}$ is the inverse temperature, and $\mathbf{w} \in \mathbb{R}^D$ is a learnable query. AP-OOD also uses attention for the corpus-wide pooling: Given the sequence representations $(\mathbf{Z}_1, \dots, \mathbf{Z}_N)$ where $\mathbf{Z}_i \in \mathcal{Z}$ from a corpus $(\mathbf{x}_1, \dots, \mathbf{x}_N)$ with $\mathbf{Z}_i := \phi_{\text{enc}}(\mathbf{x}_i)$, we define $\tilde{\mathbf{Z}} \in \mathcal{Z}$ as the concatenation of all sequence representations: $\tilde{\mathbf{Z}} := (\mathbf{Z}_1 \parallel \dots \parallel \mathbf{Z}_N)$. AP-OOD estimates $\boldsymbol{\mu} := \text{AttPool}_\beta(\tilde{\mathbf{Z}}, \mathbf{w})$. Given the $\bar{\mathbf{z}}$ and $\boldsymbol{\mu}$ from the attention pooling, AP-OOD estimates $d^2(\mathbf{Z}, \tilde{\mathbf{Z}})$, the squared distance between a sequence representation \mathbf{Z} and the concatenation $\tilde{\mathbf{Z}}$ analogous to Equation (6):

$$d^2(\mathbf{Z}, \tilde{\mathbf{Z}}) := \sum_{j=1}^M \left(\mathbf{w}_j^T \mathbf{Z} \text{softmax}(\beta \mathbf{Z}^T \mathbf{w}_j) - \mathbf{w}_j^T \tilde{\mathbf{Z}} \text{softmax}(\beta \tilde{\mathbf{Z}}^T \mathbf{w}_j) \right)^2 = \sum_{j=1}^M d_j^2(\mathbf{Z}, \tilde{\mathbf{Z}}). \quad (8)$$

We refer to $M \in \mathbb{N}$ as the number of heads. In general, M does not need to equal the embedding dimension D . We show in Appendix B.3 that, when $\beta = 0$ and $M = D$, Equation (8) reduces to the Mahalanobis distance (Equations (5) and (6)). To the best of our knowledge, AP-OOD is the first approach to integrate attention pooling into the Mahalanobis distance via a learnable directional decomposition. In Appendix B.1, we show that $s_{\min}(\mathbf{Z}) = \min_j -d_j^2(\mathbf{Z}, \tilde{\mathbf{Z}}) + \log(\|\mathbf{w}_j\|_2^2)$ is a score function as defined in Equation (2). Our score arises naturally as the upper bound

$$s(\mathbf{Z}) := \sum_{j=1}^M -d_j^2(\mathbf{Z}, \tilde{\mathbf{Z}}) + \log(\|\mathbf{w}_j\|_2^2). \quad (9)$$

In Appendix D.7, we empirically compare the min-based score $s_{\min}(\mathbf{Z})$ to its upper-bound variant $s(\mathbf{Z})$ and find that $s(\mathbf{Z})$ yields stronger OOD discrimination. The choice of this score naturally leads to the loss function of AP-OOD:

$$\mathcal{L}(\mathbf{w}_1, \dots, \mathbf{w}_M) := \frac{1}{N} \sum_{i=1}^N d^2(\mathbf{Z}_i, \tilde{\mathbf{Z}}) - \sum_{j=1}^M \log(\|\mathbf{w}_j\|_2^2). \quad (10)$$

We provide the pseudocode for AP-OOD in Algorithm 1. Scaling to large data sets requires efficient computation of $\boldsymbol{\mu} = \tilde{\mathbf{Z}} \text{softmax}(\beta \tilde{\mathbf{Z}}^T \mathbf{w})$; the naive method loads the entire concatenated sequence $\tilde{\mathbf{Z}}$ into memory, but we reduce the memory footprint by performing attention pooling on mini-batches. We describe this procedure in Appendix C.1.

Multiple queries per head. We now extend AP-OOD and use multiple queries per head. We use a set of stacked queries $\mathbf{W}_j = (\mathbf{w}_{j1}, \dots, \mathbf{w}_{jT}) \in \mathbb{R}^{D \times T}$ per head. For simplicity, we

216 consider a single head with the queries $\mathbf{W} \in \mathbb{R}^{D \times T}$ for now. We begin by extending the
 217 softmax notation from [Ramsauer et al. \(2021\)](#) to matrix-valued arguments. Given a matrix
 218 $\mathbf{A} \in \mathbb{R}^{S \times T}$

$$\text{softmax}(\beta \mathbf{A})_{st} := \frac{\exp(\beta a_{st})}{\sum_{s'=1}^S \sum_{t'=1}^T \exp(\beta a_{s't'})}. \quad (11)$$

222 In other words, the softmax normalizes over the rows and columns of \mathbf{A} . Next, we extend
 223 the attention pooling process from Equation (7) with the matrix-valued softmax: AP-
 224 OOD transforms the sequence representation $\mathbf{Z} \in \mathbb{R}^{D \times S}$ with S tokens to a new sequence
 225 representation $\tilde{\mathbf{Z}} \in \mathbb{R}^{D \times T}$ with T tokens using $\tilde{\mathbf{Z}} := \mathbf{Z}\mathbf{P}$. The updated attention pooling
 226 process is

$$\text{AttPool}_\beta(\mathbf{Z}, \mathbf{W}) := \mathbf{Z} \text{softmax}(\beta \mathbf{Z}^T \mathbf{W}) \quad \text{and} \quad \tilde{\mathbf{Z}} := \text{AttPool}_\beta(\mathbf{Z}, \mathbf{W}). \quad (12)$$

228 To the best of our knowledge, this work is the first to use a matrix-valued global softmax
 229 to transform a sequence \mathbf{Z} into another sequence $\tilde{\mathbf{Z}}$. Finally, AP-OOD uses $\mathbf{W} \in \mathbb{R}^{D \times T}$ to
 230 transform the $\tilde{\mathbf{Z}} \in \mathbb{R}^{D \times T}$ to a real number with the Frobenius inner product $\langle \mathbf{W}, \tilde{\mathbf{Z}} \rangle_F =$
 231 $\text{vec}(\mathbf{W})^T \text{vec}(\tilde{\mathbf{Z}}) = \text{Tr}(\mathbf{W}^T \tilde{\mathbf{Z}})$. To summarize, the extended squared distance is

$$233 d^2(\mathbf{Z}, \tilde{\mathbf{Z}}) := \sum_{j=1}^M \left(\text{Tr}(\mathbf{W}_j^T \mathbf{Z} \text{softmax}(\beta \mathbf{Z}^T \mathbf{W}_j)) - \text{Tr}(\mathbf{W}_j^T \tilde{\mathbf{Z}} \text{softmax}(\beta \tilde{\mathbf{Z}}^T \mathbf{W}_j)) \right)^2. \quad (13)$$

236 Finally, the regularizing term is $-\log(\|\mathbf{W}\|_F^2)$ (where $\|\cdot\|_F^2$ denotes the squared Frobenius
 237 norm). To summarize, the extended loss is

$$238 \mathcal{L}(\mathbf{W}_1, \dots, \mathbf{W}_M) := \frac{1}{N} \sum_{i=1}^N d^2(\mathbf{Z}_i, \tilde{\mathbf{Z}}) - \sum_{j=1}^M \log(\|\mathbf{W}_j\|_F^2). \quad (14)$$

241 We provide PyTorch-style pseudocode implementing Equation (14) in Appendix C.2.

244 2.2 SUPERVISED OOD DETECTION

245 **Background.** Supplying an OOD detector with information about the distribution of the
 246 OOD examples at training time can improve the ID–OOD decision boundary ([Hendrycks
 247 et al., 2018](#)). In practice, it is hard to find OOD data for training that is fully indicative
 248 of the OOD distribution seen during inference. Outlier exposure (OE; [Hendrycks et al.,
 249 2018](#)) therefore uses a large and diverse auxiliary outlier set (AUX; e.g., C4 for text data)
 250 as a stand-in for the OOD case. However, acquiring such large and diverse AUX datasets
 251 is not always possible. For example, consider a translation task with a less widely spoken
 252 source language. As another example, consider detecting defects in industrial machines using
 253 recordings of their sounds ([Nishida et al., 2024](#)). Practitioners can collect a relatively large
 254 amount of ID audio data from machines while they run without defects. However, it is
 255 much harder to collect diverse AUX examples from defective machines because defects are
 256 infrequent. In such a case, one might have to resort to a smaller AUX data set. Therefore,
 257 an OOD detector should scale gracefully with the degree of auxiliary supervision, adapting
 258 to the available number of AUX examples (e.g., [Ruff et al., 2019](#); [Liznerski et al., 2022](#);
 259 [Yoon et al., 2023](#); [Ivanov et al., 2024](#); [Qiao et al., 2024](#)).

260 **Utilizing AUX data.** To adapt AP-OOD to the supervised setting, we follow [Ruff et al.
 261 \(2019\)](#) and [Liznerski et al. \(2022\)](#): AP-OOD punishes large squared distances $d^2(\mathbf{Z}, \tilde{\mathbf{Z}})$
 262 for ID samples \mathbf{Z} and encourages large squared distances for AUX samples \mathbf{Z} . For-
 263 mally, AP-OOD minimizes the binary cross-entropy loss with the classes ID and AUX
 264 with $p(y = \text{ID} | \mathbf{Z}) = \exp(-d^2(\mathbf{Z}, \tilde{\mathbf{Z}}))$. Given N ID examples $(\mathbf{Z}_1, \dots, \mathbf{Z}_N)$, and N' AUX
 265 examples $(\mathbf{Z}_{N+1}, \dots, \mathbf{Z}_{N+N'})$, AP-OOD minimizes the supervised loss

$$267 \mathcal{L}_{\text{SUP}} := \frac{1}{N + N'} \sum_{i=1}^N d^2(\mathbf{Z}_i, \tilde{\mathbf{Z}}) - \lambda \frac{1}{N + N'} \sum_{i=N+1}^{N+N'} \log(1 - \exp(-d^2(\mathbf{Z}_i, \tilde{\mathbf{Z}}))), \quad (15)$$

268 where $\lambda \in \mathbb{R}_{\geq 0}$. If $\lambda = 0$, \mathcal{L}_{SUP} equals the unsupervised loss \mathcal{L} without the regularizing term.

270 Table 1: Unsupervised OOD detection performance on text summarization. We compare
 271 results from AP-OOD, Mahalanobis (Lee et al., 2018; Ren et al., 2023), KNN (Sun et al., 2022),
 272 Deep SVDD (Ruff et al., 2018), model perplexity (Ren et al., 2023), and entropy (Malinin &
 273 Gales, 2020) on PEGASUS_{LARGE} trained on XSUM as the ID data set. ↓ indicates “lower is
 274 better” and ↑ “higher is better”. All values in %. We estimate standard deviations across
 275 five independent data set splits and training runs.

		CNN/DM	Newsroom	Reddit	Samsun	Mean
Input OOD						
Mahalanobis	AUROC ↑	69.00 \pm 0.27	86.37 \pm 0.19	98.64 \pm 0.07	99.77 \pm 0.01	88.45
	FPR95 ↓	92.19 \pm 0.05	64.48 \pm 0.71	2.45 \pm 0.34	0.17 \pm 0.02	39.82
KNN	AUROC ↑	54.34 \pm 0.15	73.76 \pm 0.09	94.52 \pm 0.03	98.82 \pm 0.01	80.36
	FPR95 ↓	99.40 \pm 0.03	88.56 \pm 0.17	51.24 \pm 0.70	3.07 \pm 0.16	60.57
Deep SVDD	AUROC ↑	75.86 \pm 1.00	91.20 \pm 0.21	99.73 \pm 0.05	99.57 \pm 0.04	91.59
	FPR95 ↓	73.70 \pm 2.35	36.46 \pm 1.12	0.26 \pm 0.09	0.67 \pm 0.17	27.77
AP-OOD (Ours)	AUROC ↑	96.13 \pm 0.44	99.10 \pm 0.08	99.91 \pm 0.03	99.80 \pm 0.04	98.74
	FPR95 ↓	19.51 \pm 2.24	4.11 \pm 0.28	0.00 \pm 0.01	0.04 \pm 0.03	5.91
Output OOD						
Perplexity	AUROC ↑	42.20 \pm 0.14	53.99 \pm 0.31	83.38 \pm 0.15	78.53 \pm 0.31	64.52
	FPR95 ↓	77.71 \pm 0.17	79.07 \pm 0.57	45.56 \pm 0.40	46.96 \pm 0.20	62.32
Entropy	AUROC ↑	59.59 \pm 0.21	77.20 \pm 0.52	93.47 \pm 0.21	87.17 \pm 0.20	79.36
	FPR95 ↓	79.04 \pm 0.75	64.24 \pm 1.21	30.19 \pm 1.34	50.47 \pm 1.64	55.98
Mahalanobis	AUROC ↑	63.27 \pm 0.17	88.26 \pm 0.11	97.40 \pm 0.09	97.29 \pm 0.08	86.55
	FPR95 ↓	89.84 \pm 0.13	47.83 \pm 0.71	11.13 \pm 0.58	13.57 \pm 0.25	40.59
KNN	AUROC ↑	74.37 \pm 0.13	86.96 \pm 0.08	95.85 \pm 0.06	97.33 \pm 0.03	88.63
	FPR95 ↓	73.36 \pm 0.20	53.44 \pm 0.58	15.78 \pm 0.27	10.29 \pm 0.22	38.22
Deep SVDD	AUROC ↑	68.31 \pm 1.63	94.13 \pm 0.12	97.60 \pm 0.26	95.97 \pm 0.15	89.00
	FPR95 ↓	76.76 \pm 1.15	19.22 \pm 0.34	8.90 \pm 1.25	20.17 \pm 1.28	31.26
AP-OOD (Ours)	AUROC ↑	93.37 \pm 0.54	92.62 \pm 0.67	98.04 \pm 0.28	98.30 \pm 0.11	95.59
	FPR95 ↓	23.12 \pm 1.97	29.91 \pm 2.93	6.34 \pm 1.56	6.83 \pm 0.64	16.55

3 EXPERIMENTS

296 **Toy experiment.** We present a toy experiment illustrating the main intuitions behind
 297 AP-OOD. Figure 1 demonstrates a simple failure mode of mean pooling approaches: First, we
 298 generate ID and OOD token embeddings $\mathbf{Z}_i \in \mathbb{R}^{2 \times 2}$. Each ID sequence representation consists
 299 of one token sampled from $\mathcal{N}((1, 1), \sigma^2 \mathbf{I})$ (where $\sigma := 0.1$) and one token sampled from
 300 $\mathcal{N}((-1, -1), \sigma^2 \mathbf{I})$. The OOD sequences contain two tokens sampled from $\mathcal{N}((-1, 1), \sigma^2 \mathbf{I})$
 301 and $\mathcal{N}((1, -1), \sigma^2 \mathbf{I})$, respectively. The left panel shows the generated sequences, where each
 302 sequence consists of two dots (representing the two tokens) connected by a line. Because
 303 the means of the ID and OOD sequences both cluster around the origin (central panel), the
 304 Mahalanobis distance with mean pooling fails to discriminate between them (right panel).
 305 Figure 2 shows how AP-OOD overcomes this limitation: We set $M = 1$ and $T = 1$ and
 306 train AP-OOD as described in Section 2.1 on the ID data only, but we modify the pooling
 307 mechanism from Equation (7): We replace the dot product similarity in the softmax with
 308 the negative squared Euclidean distance, as it is known to work better in low-dimensional
 309 spaces (we provide the formal definition for this modification in Appendix D.1). The left
 310 panel of Figure 2 shows that the loss landscape of \mathbf{w} forms two basins at the locations of the
 311 ID tokens. The central panel shows that after training, \mathbf{w} is located in one of the basins.
 312 Finally, the right panel shows that AP-OOD perfectly discriminates ID and OOD.

313 **Summarization.** We follow Ren et al. (2023) and use a PEGASUS_{LARGE} (Zhang et al.,
 314 2020) fine-tuned on the ID data set XSUM (Narayan et al., 2018). We utilize the C4 training
 315 split as the AUX data set. We measure the OOD detection performance on the data sets
 316 CNN/Daily Mail (CNN/DM; news articles from CNN and Daily Mail; Hermann et al., 2015;
 317 See et al., 2017), Newsroom (articles and summaries written by authors and editors from 38
 318 news publications; Grusky et al., 2018), Reddit TIFU (posts and summaries from the online
 319 discussion forum Reddit; Kim et al., 2018), and Samsun (summaries of casual dialogues;
 320 Gliwa et al., 2019). The ForumSum data set used in the experiments of Ren et al. (2023)
 321 has been retracted. Therefore, we do not use it in our experiments.

322 **Translation.** We train a Transformer (base) on WMT15 En–Fr (Bojar et al., 2015). The
 323 model trains for 100,000 steps using AdamW (Loshchilov & Hutter, 2017) with a cosine
 324 schedule (Loshchilov & Hutter, 2016), linear warmup, and a peak learning rate of 5×10^{-4} .

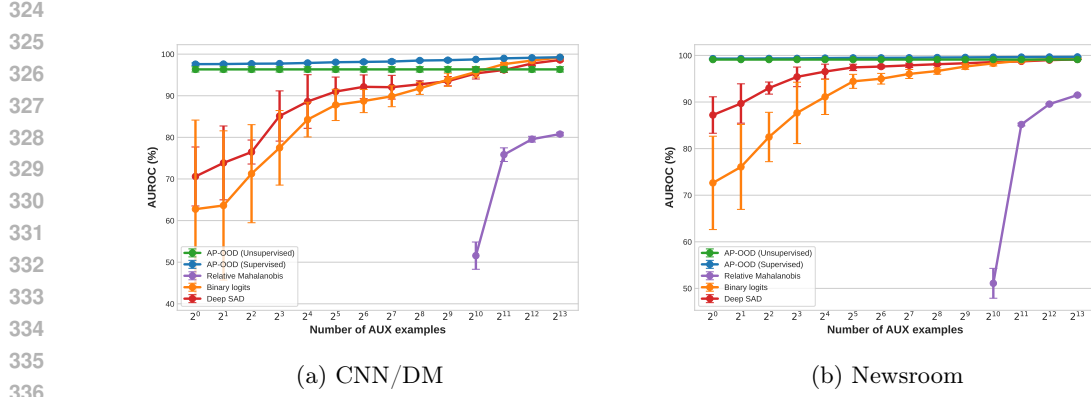


Figure 3: OOD detection performance on the input token embeddings of PEGASUS_{LARGE} trained on XSUM. We vary the number of AUX samples and compare AP-OOD, binary logits (Ren et al., 2023), Deep SAD (Ruff et al., 2019), and relative Mahalanobis (Ren et al., 2023). AP-OOD attains the highest AUROC independent of AUX sample count.

We set the batch size to 1024 and the context length to 512. Following Ren et al. (2023), the AUX data set is ParaCrawl En-Fr, and the OOD data sets are newstest2014 (nt2014), newsdiscussdev2015 (ddd2015), and newsdiscusstest2015 (ndt2015) from WMT15 (Bojar et al., 2015), and the Law, Koran, Medical, IT, and Subtitles subsets from OPUS (Tiedemann, 2012; Aulamo & Tiedemann, 2019).

Training. We extract 100,000 ID sequence representations (\mathbf{E} or \mathbf{G}) and use all extracted representations for training AP-OOD in all experiments. We also extract AUX sequence representations, and we vary the number of AUX sequences available from 0 (unsupervised) to 10,000 (fully supervised). While training AP-OOD, the transformer model remains frozen. We use the Adam optimizer (Kingma & Ba, 2014) without weight decay, set the learning rate to 0.01, and apply a cosine schedule (Loshchilov & Hutter, 2016). We train for 2,000 steps with a batch size of 512. We select M and T such that the parameter count of AP-OOD matches the parameter count of the Mahalanobis method (i.e., the size of Σ). For more information on hyperparameter selection, we refer to Appendix D.2. An additional scaling experiment on input sequence representations of the summarization task investigates larger parameter spaces: We train on the full XSUM data set (instead of the 100,000 ID sequence representations used in the other experiments). We select the number of heads (M) from the set {1, 16, 128, 1024}, the number of queries (T) from the set {1, 4, 16}, and β from {1/ \sqrt{D} , 0.25, 0.5, 1, 2}. The largest configuration has a parameter count 16 times greater than the Mahalanobis baseline.

Baselines. We compare AP-OOD to six unsupervised OOD detection methods: We apply the embedding-based methods Mahalanobis (Lee et al., 2018; Ren et al., 2023), KNN (Sun et al., 2022), and Deep SVDD (Ruff et al., 2018) to both the input and output sequence representations (\mathbf{E} and \mathbf{G} , respectively), and we apply Perplexity (Ren et al., 2023) and Entropy (Malinin & Gales, 2020) to the output of the decoder. We also compare AP-OOD to three supervised OOD detection methods: binary logits (Ren et al., 2023), relative Mahalanobis (Ren et al., 2023), and Deep SVDD (Ruff et al., 2019). We evaluate the discriminative power of the methods in our comparison using the false positive rate at 95% true positives (FPR95) and AUROC.

Audio data. To demonstrate the effectiveness of AP-OOD on data modalities other than text, we apply the method to the MIMII-DG audio data set (Dohi et al., 2022). The data set comprises audio recordings of 15 different machines, ranging from 10 to 12 seconds in length. The dataset contains 990 samples per machine. During preprocessing, the raw audio waveforms are converted into audio spectrograms. We train a transformer to classify a subset of 7 machines. The remaining 8 machines are considered as OOD. The architecture and training method for the network were adopted from Huang et al. (2022). To adjust for the

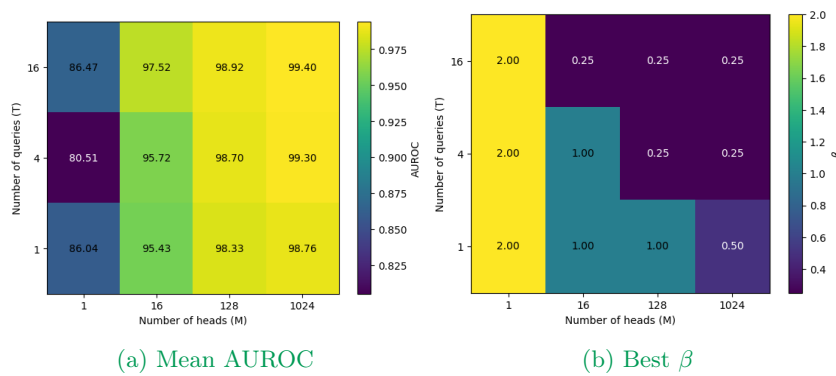


Figure 4: OOD detection performance on the input token embeddings of PEGASUS_{LARGE} trained on XSUM when scaling to large M and T . We vary $M \in \{1, 16, 128, 1024\}$, $T \in \{1, 4, 16\}$, and $\beta \in \{1/\sqrt{D}, 0.25, 0.5, 1, 2\}$. **(Left)** Mean AUROC in % for the best β at each (M, T) combination. **(Right)** The best β selected at each (M, T) combination.

small data set size, we decrease the size of the architecture: We increase the patch size to 32×32 pixels, decrease the embedding dimension to 32, and utilize only three attention blocks with four heads each. Consequently, the encoder of the network produces 128 tokens with $D = 32$ features. We train AP-OOD on the encoder output in the unsupervised setting using $M = 128$ and $T = 8$.

4 RESULTS

Table 1 shows the results on unsupervised OOD detection on the text summarization task. AP-OOD surpasses methods with mean pooling by a large margin for both input and output settings for most OOD data sets. Most notably, the mean FPR95 on CNN/DM improves from 73.70% for the best baseline Deep SVDD to 19.51% for AP-OOD. The table also shows that the embedding-based methods (Mahalanobis, KNN, Deep SVDD, and AP-OOD) perform better than the prediction-based baselines perplexity and entropy. Figure 3 shows the results of AP-OOD in the semi-supervised setting: supplying AUX data to AP-OOD improves the AUROC, and more AUX data results in a larger improvement. AP-OOD attains the highest AUROC independent of AUX sample count. We include the results on additional OOD data sets in the semi-supervised setting and results on fully supervised OOD detection on the summarization task in Appendix D.3, and we present ablations on AP-OOD on text summarization in Appendix D.8.

Figure 4 shows the results when scaling AP-OOD to larger parameter counts. As we increase the number of heads (M) and queries (T), we observe a steady increase in the mean AUROC on the summarization task. The highest Mean AUROC of 99.40% is achieved by the largest configuration tested ($M = 1024$, $T = 16$).

Table 2 shows the results on unsupervised OOD detection on the translation task. AP-OOD gives the best average results for the input and output settings. It is noteworthy that in the translation task, the prediction-based methods perform better, with the perplexity baseline outperforming all embedding-based methods evaluated on the output token embeddings except AP-OOD. We hypothesize that this discrepancy can be explained as follows: In translation, ID uncertainty is typically low because the source sentence largely dictates what must be generated — specific words, names, and inflections — so ID perplexities are small and tightly clustered. In text summarization, ID uncertainty is higher because many different summaries can be equally valid, with freedom in what to include and how to phrase it. This raises and spreads ID perplexity and weakens ID–OOD separation when using perplexity. We include results on fully supervised OOD detection for translation in Appendix D.5. Furthermore, we verify the effectiveness of AP-OOD on the decoder-only language modeling paradigm using Pythia-160M in Appendix D.6.

432 Table 2: Unsupervised OOD detection performance on English-to-French translation. We
 433 compare results from AP-OOD, Mahalanobis (Lee et al., 2018; Ren et al., 2023), KNN (Sun
 434 et al., 2022), Deep SVDD (Ruff et al., 2018), model perplexity (Ren et al., 2023), and
 435 entropy (Malinin & Gales, 2020) on a Transformer (base) trained on WMT15 En-Fr as the
 436 ID data set. ↓ indicates “lower is better” and ↑ “higher is better”. All values in %. We
 437 estimate standard deviations across five independent data set splits and training runs.

		IT	Koran	Law	Medical	Subtitles	ndd2015	ndt2015	nt2014	Mean
Input OOD										
Mahalanobis	AUROC ↑	93.94 \pm 0.01	66.82 \pm 0.29	49.39 \pm 0.30	78.50 \pm 0.41	89.61 \pm 0.09	65.87 \pm 0.01	66.44 \pm 0.01	51.53 \pm 0.01	70.26
	FPR95 ↓	31.29 \pm 0.29	93.46 \pm 0.27	91.26 \pm 0.50	63.13 \pm 0.77	59.60 \pm 0.48	87.01 \pm 0.14	89.09 \pm 0.10	97.13 \pm 0.10	76.50
KNN	AUROC ↑	94.16 \pm 0.01	66.16 \pm 0.24	46.68 \pm 0.22	79.62 \pm 0.41	89.16 \pm 0.11	64.81 \pm 0.05	65.63 \pm 0.05	53.21 \pm 0.05	69.93
	FPR95 ↓	32.44 \pm 0.12	94.69 \pm 0.28	92.71 \pm 0.34	67.04 \pm 0.73	63.35 \pm 0.32	88.01 \pm 0.07	89.97 \pm 0.04	97.51 \pm 0.03	78.33
Deep SVDD	AUROC ↑	92.53 \pm 0.15	64.12 \pm 0.81	51.56 \pm 1.21	77.40 \pm 0.52	87.64 \pm 0.37	63.30 \pm 0.40	63.58 \pm 0.31	49.31 \pm 0.31	68.68
	FPR95 ↓	39.37 \pm 0.94	95.24 \pm 0.28	92.80 \pm 0.29	66.17 \pm 0.71	65.53 \pm 1.33	89.87 \pm 0.22	90.91 \pm 0.27	98.07 \pm 0.19	79.74
AP-OOD (Ours)	AUROC ↑	94.88 \pm 0.08	73.51 \pm 0.33	51.11 \pm 0.38	81.80 \pm 0.35	89.14 \pm 0.32	69.98 \pm 0.15	70.40 \pm 0.27	57.82 \pm 0.23	73.58
	FPR95 ↓	25.00 \pm 0.59	87.48 \pm 0.33	89.45 \pm 0.67	58.51 \pm 0.60	60.78 \pm 2.07	86.45 \pm 0.91	87.05 \pm 0.32	94.19 \pm 0.41	73.61
Output OOD										
Perplexity	AUROC ↑	94.06 \pm 0.00	77.05 \pm 0.20	45.18 \pm 0.38	75.41 \pm 0.42	92.38 \pm 0.08	75.32 \pm 0.02	75.81 \pm 0.02	61.74 \pm 0.02	74.62
	FPR95 ↓	35.36 \pm 0.01	90.54 \pm 0.35	90.14 \pm 0.34	69.17 \pm 0.60	50.11 \pm 0.58	83.94 \pm 0.04	85.47 \pm 0.00	96.80 \pm 0.00	75.19
Entropy	AUROC ↑	71.44 \pm 0.22	86.14 \pm 0.32	53.98 \pm 0.23	51.12 \pm 0.44	70.95 \pm 0.47	75.11 \pm 0.96	72.96 \pm 0.22	71.31 \pm 0.17	69.13
	FPR95 ↓	71.19 \pm 0.95	56.19 \pm 1.91	93.94 \pm 0.37	90.27 \pm 0.64	74.56 \pm 1.23	76.28 \pm 2.13	77.65 \pm 1.54	85.71 \pm 1.32	78.23
Mahalanobis	AUROC ↑	90.74 \pm 0.01	69.38 \pm 0.17	52.25 \pm 0.14	75.68 \pm 0.47	86.57 \pm 0.08	62.28 \pm 0.03	62.76 \pm 0.02	48.63 \pm 0.02	68.54
	FPR95 ↓	57.02 \pm 0.44	94.26 \pm 0.23	97.15 \pm 0.15	81.34 \pm 0.33	76.16 \pm 0.79	93.09 \pm 0.29	93.93 \pm 0.13	98.00 \pm 0.09	86.37
KNN	AUROC ↑	95.35 \pm 0.04	71.55 \pm 0.17	57.40 \pm 0.14	78.53 \pm 0.58	87.06 \pm 0.12	67.16 \pm 0.12	67.90 \pm 0.13	58.38 \pm 0.10	72.92
	FPR95 ↓	27.61 \pm 0.31	94.13 \pm 0.11	93.82 \pm 0.32	65.10 \pm 0.58	72.73 \pm 0.43	91.33 \pm 0.08	91.88 \pm 0.10	96.79 \pm 0.05	79.17
Deep SVDD	AUROC ↑	89.20 \pm 0.13	67.28 \pm 0.80	54.40 \pm 0.83	73.96 \pm 0.65	84.00 \pm 0.19	60.37 \pm 0.57	60.66 \pm 0.37	47.11 \pm 0.22	67.12
	FPR95 ↓	62.41 \pm 1.21	95.19 \pm 0.48	95.03 \pm 0.65	81.50 \pm 1.69	81.56 \pm 1.15	93.93 \pm 0.26	95.75 \pm 0.44	98.41 \pm 0.16	87.97
AP-OOD (Ours)	AUROC ↑	96.28 \pm 0.11	80.70 \pm 0.50	53.07 \pm 0.68	80.84 \pm 0.87	93.88 \pm 0.36	80.64 \pm 0.57	81.39 \pm 0.56	68.12 \pm 0.65	79.36
	FPR95 ↓	21.20 \pm 0.65	82.49 \pm 1.29	87.38 \pm 0.44	63.67 \pm 1.03	40.27 \pm 3.02	77.14 \pm 1.68	78.39 \pm 1.29	94.50 \pm 0.40	68.13

454 Table 3: Unsupervised OOD detection performance on audio classification. We compare
 455 results from AP-OOD, Mahalanobis (Lee et al., 2018; Ren et al., 2023), KNN (Sun et al.,
 456 2022), Deep SVDD (Ruff et al., 2018), MSP (Hendrycks & Gimpel, 2016), and EBO (Liu
 457 et al., 2020b) trained on MIMII-DG (Dohi et al., 2022) as the ID data set. ↓ indicates “lower
 458 is better” and ↑ “higher is better”. All values in %. We estimate standard deviations across
 459 five independent training runs.

	Mahalanobis	KNN	Deep SVDD	MSP	EBO	AP-OOD (Ours)
AUROC ↑	64.96 \pm 0.002	81.21 \pm 0.000	53.48 \pm 1.930	88.05 \pm 0.000	90.75 \pm 0.000	92.86\pm0.746
FPR95 ↓	84.39 \pm 0.011	57.11 \pm 0.000	89.44 \pm 1.689	36.43 \pm 0.000	61.86 \pm 0.000	22.35\pm2.388

464 In the audio task, the network achieves an accuracy of 97.6% on the primary classification
 465 task. Table 3 presents the results of the unsupervised OOD detection methods AP-OOD,
 466 Mahalanobis (Lee et al., 2018), KNN (Sun et al., 2022), and Deep SVDD (Ruff et al.,
 467 2018). Additionally, we compare AP-OOD to 2 methods for classifiers, Maximum Softmax
 468 Probability (MSP; Hendrycks & Gimpel, 2016) and Energy-based OOD Detection (EBO;
 469 Liu et al., 2020b). In contrast to the other methods, MSP and EBO do not apply to
 470 transformer tokens, making them unsuitable for summarization and translation tasks. The
 471 results show that AP-OOD improves the FPR95 metric from 36.43% (MSP) to 22.35%.

472 We evaluate the runtime performance of AP-OOD by measuring the inference time of
 473 single batches on the summarization task. We find that while AP-OOD is slower than
 474 the Mahalanobis baseline, it is still substantially faster than a forward pass through the
 475 transformer encoder. Because AP-OOD rejects a larger portion of OOD examples, the
 476 avoided generation time can effectively offset the AP-OOD’s computational overhead relative
 477 to the baseline. For more details on the runtime behavior, we refer to Appendix D.9.

5 RELATED WORK

481 **OOD detection.** Some authors (e.g., Bishop, 1994; Roth et al., 2022; Yang et al., 2022)
 482 distinguish between anomalies, outliers, and novelties. These distinctions reflect different
 483 goals within applications (Ruff et al., 2021). For example, when an anomaly is found, it will
 484 usually be removed from the training pipeline. However, when a novelty is found, it should
 485 be studied. We focus on detecting samples that are not part of the training distribution
 486 and consider sample categorization as a downstream task. OOD detection methods can be

486 categorized into three groups: Post-hoc, training-time, and OE methods. In the post-hoc
 487 approach, one employs statistics obtained from a classifier. Perhaps the most well-known
 488 approach is the maximum softmax probability (MSP; [Hendrycks & Gimpel, 2016](#)). A wide
 489 range of post-hoc OOD detection approaches have been proposed to address the shortcomings
 490 of MSP (e.g., [Lee et al., 2018](#); [Hendrycks et al., 2019a](#); [Liu et al., 2020a](#); [Sun et al., 2021](#);
 491 [2022](#); [Wang et al., 2022](#); [Zhang et al., 2023b](#); [Djurisic et al., 2023](#); [Liu et al., 2023](#); [Xu et al.,](#)
 492 [2024](#); [Guo et al., 2025](#)). A commonly used post-hoc method is the Mahalanobis distance
 493 (e.g., [Lee et al., 2018](#); [Sehwag et al., 2021](#); [Ren et al., 2023](#)). Recently, [Müller & Hein \(2025\)](#)
 494 proposed feature normalization to improve Mahalanobis-based OOD detection, and [Guo et al.](#)
 495 ([2025](#)) show that the Mahalanobis distance benefits from dynamically adjusting the prior
 496 geometry in response to new data. In contrast to post-hoc methods, training-time methods
 497 modify the training process of the encoder (e.g., [Hendrycks et al., 2019c](#); [Sehwag et al.,](#)
 498 [2021](#); [Du et al., 2022](#); [Hendrycks et al., 2022](#); [Ming et al., 2023](#); [Tao et al., 2023](#); [Lu et al.,](#)
 499 [2024](#)). Finally, the group of OE methods incorporates AUX data in the training process
 500 (e.g., [Hendrycks et al., 2019b](#); [Liu et al., 2020a](#); [Ming et al., 2022](#); [Zhang et al., 2023a](#); [Wang](#)
 501 [et al., 2023](#); [Zhu et al., 2023](#); [Jiang et al., 2024](#); [Hofmann et al., 2024](#)).

502 **OOD detection and natural language.** Most of the aforementioned OOD detection
 503 approaches target vision tasks, and many of them require a classification model as the encoder
 504 ϕ . Applying these vision-based OOD methods to text is not straightforward due to the
 505 sequence-dependent nature of natural language (e.g., in autoregressive language generation).
 506 OOD detection specifically tailored for natural language is still underexplored. [Ren et al.](#)
 507 ([2023](#)) propose the log-model perplexity of a generated sequence \mathbf{y} as a simple baseline
 508 for OOD detection on autoregressive language modeling tasks: $-\frac{1}{L} \sum_{l=1}^L \log p_\theta(y_l | \mathbf{y}_{<l}, \mathbf{x})$.
 509 However, they show experimentally that model perplexity is inherently limited. Because of
 510 these shortcomings, [Ren et al. \(2023\)](#) propose embedding-based OOD detection methods for
 511 text data. Relatively few other works have explored OOD detection for generative language
 512 modeling. Notable applications include translation (e.g., [Xiao et al., 2020](#); [Malinin et al.,](#)
 513 [2021](#); [Ren et al., 2023](#)), summarization ([Ren et al., 2023](#)), and mathematical reasoning ([Wang](#)
 514 [et al., 2024](#)). A related field is hallucination detection (e.g., [Malinin & Gales, 2020](#); [Farquhar](#)
 515 [et al., 2024](#); [Du et al., 2024](#); [Aichberger et al., 2025](#); [Park et al., 2025](#)). Unlike OOD detection
 516 (which flags inputs outside the training distribution), the goal of hallucination detection is
 517 to identify prompts a generative language model is unlikely to answer truthfully.

518 6 LIMITATIONS & FUTURE WORK

520 We would like to discuss two limitations that we found. First, the selection of the AUX
 521 data is crucial, since it determines the shape of the ID–OOD decision boundary. If the AUX
 522 distribution diverges from the OOD examples faced at inference, the induced boundary may
 523 not be aligned with the task. Second, it remains unclear how reliably the OOD detection
 524 performance on specific data sets can indicate the general ability to detect OOD examples, as
 525 a large portion of plausible OOD inputs remains untested. An interesting avenue for future
 526 work is to apply OOD detection methods to large language models (LLMs; e.g., [Abdin](#)
 527 [et al., 2024](#); [Dubey et al., 2024](#); [Yang et al., 2025](#)). While we demonstrate the applicability of
 528 AP-OOD on the decoder-only language modeling paradigm of LLMs (Appendix D.6), further
 529 challenges include proprietary training data, finding OOD data for training and evaluation
 530 given the breadth of the ID data, and the ambiguity of p_{ID} arising from complex training
 531 pipelines involving multiple phases (e.g., [Wei et al., 2022](#); [Ouyang et al., 2022](#)).

532 7 CONCLUSION

533 We introduce AP-OOD: an approach for OOD detection for natural language that can learn
 534 in supervised and unsupervised settings. In contrast to previous methods, AP-OOD learns
 535 how to pool token-level information without the explicit need for AUX data. Our experiments
 536 show that when supplied with AUX data during training, the performance of AP-OOD
 537 improves as more AUX data is provided. We compare AP-OOD to five unsupervised and
 538 three supervised OOD detection methods. Overall, AP-OOD shows the best results.

540 REPRODUCIBILITY STATEMENT
541

542 To ensure reproducibility, we provide the source code of our implementation of AP-OOD in the
543 unsupervised and supervised settings in the supplementary material. Detailed instructions on
544 running the source code and reproducing the experiments are provided in the file `readme.md`.
545 We provide information about data, the training process, and the hyperparameter selection
546 in Section 3 and Appendix D.2.

548 REFERENCES
549

550 Marah Abdin, Jyoti Aneja, Harkirat Behl, Sébastien Bubeck, Ronen Eldan, Suriya Gunasekar,
551 Michael Harrison, Russell J Hewett, Mojan Javaheripi, Piero Kauffmann, et al. Phi-4
552 technical report. *arXiv preprint arXiv:2412.08905*, 2024.

553 Lukas Aichberger, Kajetan Schweigofer, Mykyta Ielanskyi, and Sepp Hochreiter. Improving
554 uncertainty estimation through semantically diverse language generation. In *The Thirteenth*
555 *International Conference on Learning Representations*, 2025.

556 Ghadi S Al Hajj, Aliaksandr Hubin, Chakravarthi Kanduri, Milena Pavlovic, Knut Dagestad
557 Rand, Michael Widrich, Anne Schistad Solberg, Victor Greiff, Johan Pensar, Günter
558 Klambauer, et al. Incorporating probabilistic domain knowledge into deep multiple
559 instance learning. In *Forty-first International Conference on Machine Learning*, 2024.

560 Stuart Andrews, Ioannis Tsachantaridis, and Thomas Hofmann. Support vector machines for
561 multiple-instance learning. *Advances in neural information processing systems*, 15, 2002.

562 Andreas Auer, Martin Gauch, Daniel Klotz, and Sepp Hochreiter. Conformal prediction for
563 time series with modern hopfield networks. *Advances in Neural Information Processing
564 Systems*, 36:56027–56074, 2023.

565 Mikko Aulamo and Jörg Tiedemann. The OPUS resource repository: An open package
566 for creating parallel corpora and machine translation services. In Mareike Hartmann
567 and Barbara Plank (eds.), *Proceedings of the 22nd Nordic Conference on Computational
568 Linguistics*, pp. 389–394, Turku, Finland, September–October 2019. Linköping University
569 Electronic Press.

570 Dzmitry Bahdanau. Neural machine translation by jointly learning to align and translate.
571 *arXiv preprint arXiv:1409.0473*, 2014.

572 Stella Biderman, Hailey Schoelkopf, Quentin Gregory Anthony, Herbie Bradley, Kyle O’Brien,
573 Eric Hallahan, Mohammad Aflah Khan, Shivanshu Purohit, USVSN Sai Prashanth, Edward
574 Raff, et al. Pythia: A suite for analyzing large language models across training and scaling.
575 In *International Conference on Machine Learning*, pp. 2397–2430. PMLR, 2023.

576 Christopher M Bishop. Novelty detection and neural network validation. *IEE Proceedings-
577 Vision, Image and Signal processing*, 141(4):217–222, 1994.

578 Ondřej Bojar, Rajen Chatterjee, Christian Federmann, Barry Haddow, Matthias Huck, Chris
579 Hokamp, Philipp Koehn, Varvara Logacheva, Christof Monz, Matteo Negri, Matt Post,
580 Carolina Scarton, Lucia Specia, and Marco Turchi. Findings of the 2015 workshop on
581 statistical machine translation. In Ondřej Bojar, Rajen Chatterjee, Christian Federmann,
582 Barry Haddow, Chris Hokamp, Matthias Huck, Varvara Logacheva, and Pavel Pecina
583 (eds.), *Proceedings of the Tenth Workshop on Statistical Machine Translation*, pp. 1–46,
584 Lisbon, Portugal, September 2015. Association for Computational Linguistics.

585 Thomas G Dietterich, Richard H Lathrop, and Tomás Lozano-Pérez. Solving the multiple
586 instance problem with axis-parallel rectangles. *Artificial intelligence*, 89(1-2):31–71, 1997.

587 Andrija Djurisic, Nebojsa Bozanic, Arjun Ashok, and Rosanne Liu. Extremely simple activation
588 shaping for out-of-distribution detection. In *The Eleventh International Conference
589 on Learning Representations*, 2023.

594 Kota Dohi, Tomoya Nishida, Harsh Purohit, Ryo Tanabe, Takashi Endo, Masaaki Yamamoto,
 595 Yuki Nikaido, and Yohei Kawaguchi. MIMII DG: Sound dataset for malfunctioning
 596 industrial machine investigation and inspection for domain generalization task. In *Proceedings*
 597 *of the 7th Detection and Classification of Acoustic Scenes and Events 2022 Workshop*
 598 (*DCASE2022*), Nancy, France, November 2022.

599

600 Xuefeng Du, Zhaoning Wang, Mu Cai, and Yixuan Li. Vos: Learning what you don't know
 601 by virtual outlier synthesis. *arXiv preprint arXiv:2202.01197*, 2022.

602 Xuefeng Du, Chaowei Xiao, and Sharon Li. Haloscope: Harnessing unlabeled llm generations
 603 for hallucination detection. *Advances in Neural Information Processing Systems*, 37:
 604 102948–102972, 2024.

605

606 Abhimanyu Dubey, Abhinav Jauhri, Abhinav Pandey, Abhishek Kadian, Ahmad Al-Dahle,
 607 Aiesha Letman, Akhil Mathur, Alan Schelten, Amy Yang, Angela Fan, et al. The llama 3
 608 herd of models. *arXiv e-prints*, pp. arXiv–2407, 2024.

609 Sebastian Farquhar, Jannik Kossen, Lorenz Kuhn, and Yarin Gal. Detecting hallucinations
 610 in large language models using semantic entropy. *Nature*, 630(8017):625–630, 2024.

611

612 Andreas Fürst, Elisabeth Rumetschofer, Johannes Lehner, Viet T Tran, Fei Tang, Hubert
 613 Ramsauer, David Kreil, Michael Kopp, Günter Klambauer, Angela Bitto, et al. CLOOB:
 614 Modern Hopfield networks with InfoLOOB outperform clip. *Advances in neural information*
 615 *processing systems*, 35:20450–20468, 2022.

616

617 Leo Gao, Stella Biderman, Sid Black, Laurence Golding, Travis Hoppe, Charles Foster, Jason
 618 Phang, Horace He, Anish Thite, Noa Nabeshima, et al. The pile: An 800gb dataset of
 619 diverse text for language modeling. *arXiv preprint arXiv:2101.00027*, 2020.

620

621 Bogdan Gliwa, Iwona Mochol, Maciej Biesek, and Aleksander Wawer. Samsum corpus:
 622 A human-annotated dialogue dataset for abstractive summarization. *arXiv preprint*
 623 *arXiv:1911.12237*, 2019.

624

625 Ary L Goldberger, Luis AN Amaral, Leon Glass, Jeffrey M Hausdorff, Plamen Ch Ivanov,
 626 Roger G Mark, Joseph E Mietus, George B Moody, Chung-Kang Peng, and H Eugene
 627 Stanley. Physiobank, physiotoolkit, and physionet: components of a new research resource
 628 for complex physiologic signals. *circulation*, 101(23):e215–e220, 2000.

629

630 Max Grusky, Mor Naaman, and Yoav Artzi. Newsroom: A dataset of 1.3 million summaries
 631 with diverse extractive strategies. *arXiv preprint arXiv:1804.11283*, 2018.

632

633 Kaiyu Guo, Zijian Wang, Tan Pan, Brian C Lovell, and Mahsa Baktashmotagh. Improv-
 634 ing out-of-distribution detection via dynamic covariance calibration. In *Forty-second*
 635 *International Conference on Machine Learning*, 2025.

636

637 Dan Hendrycks and Kevin Gimpel. A baseline for detecting misclassified and out-of-
 638 distribution examples in neural networks. *arXiv preprint arXiv:1610.02136*, 2016.

639

640 Dan Hendrycks, Mantas Mazeika, and Thomas Dietterich. Deep anomaly detection with
 641 outlier exposure. *arXiv preprint arXiv:1812.04606*, 2018.

642

643 Dan Hendrycks, Steven Basart, Mantas Mazeika, Andy Zou, Joe Kwon, Mohammadreza
 644 Mostajabi, Jacob Steinhardt, and Dawn Song. Scaling out-of-distribution detection for
 645 real-world settings. *arXiv preprint arXiv:1911.11132*, 2019a.

646

647 Dan Hendrycks, Mantas Mazeika, and Thomas Dietterich. Deep anomaly detection with
 648 outlier exposure. In *International Conference on Learning Representations*, 2019b. URL
 649 <https://openreview.net/forum?id=HyxCxhRcY7>.

650

651 Dan Hendrycks, Mantas Mazeika, Saurav Kadavath, and Dawn Song. Using self-supervised
 652 learning can improve model robustness and uncertainty. *Advances in neural information*
 653 *processing systems*, 32, 2019c.

648 Dan Hendrycks, Andy Zou, Mantas Mazeika, Leonard Tang, Bo Li, Dawn Song, and Jacob
 649 Steinhardt. Pixmix: Dreamlike pictures comprehensively improve safety measures. In
 650 *Proceedings of the IEEE/CVF Conference on Computer Vision and Pattern Recognition*,
 651 pp. 16783–16792, 2022.

652 Karl Moritz Hermann, Tomas Kociský, Edward Grefenstette, Lasse Espeholt, Will Kay,
 653 Mustafa Suleyman, and Phil Blunsom. Teaching machines to read and comprehend.
 654 *Advances in neural information processing systems*, 28, 2015.

655 Claus Hofmann, Simon Schmid, Bernhard Lehner, Daniel Klotz, and Sepp Hochreiter. Energy-
 656 based hopfield boosting for out-of-distribution detection. *arXiv preprint arXiv:2405.08766*,
 657 2024.

658 J. J. Hopfield. Neurons with graded response have collective computational properties like
 659 those of two-state neurons. *Proceedings of the National Academy of Sciences*, 81(10):
 660 3088–3092, 1984. doi: 10.1073/pnas.81.10.3088.

661 Po-Yao Huang, Hu Xu, Juncheng Li, Alexei Baevski, Michael Auli, Wojciech Galuba, Florian
 662 Metze, and Christoph Feichtenhofer. Masked autoencoders that listen. In *NeurIPS*, 2022.

663 Rui Huang, Andrew Geng, and Yixuan Li. On the importance of gradients for detecting
 664 distributional shifts in the wild. *Advances in Neural Information Processing Systems*, 34:
 665 677–689, 2021.

666 Maximilian Ilse, Jakub Tomczak, and Max Welling. Attention-based deep multiple instance
 667 learning. In *International conference on machine learning*, pp. 2127–2136. PMLR, 2018.

668 Viktor Ivanov, Maurizio Scaramuzza, and Richard C Wilson. Deep temporal semi-supervised
 669 one-class classification for gnss radio frequency interference detection. *The Journal of
 670 Navigation*, 77(1):59–81, 2024.

671 Wenyu Jiang, Hao Cheng, MingCai Chen, Chongjun Wang, and Hongxin Wei. DOS:
 672 Diverse outlier sampling for out-of-distribution detection. In *The Twelfth International
 673 Conference on Learning Representations*, 2024. URL <https://openreview.net/forum?id=iriEqxFB4y>.

674 Byeongchang Kim, Hyunwoo Kim, and Gunhee Kim. Abstractive summarization of reddit
 675 posts with multi-level memory networks. *arXiv preprint arXiv:1811.00783*, 2018.

676 Diederik P Kingma and Jimmy Ba. Adam: A method for stochastic optimization. *arXiv
 677 preprint arXiv:1412.6980*, 2014.

678 Balaji Lakshminarayanan, Alexander Pritzel, and Charles Blundell. Simple and scalable
 679 predictive uncertainty estimation using deep ensembles. In *Advances in Neural Information
 680 Processing Systems*, volume 30, pp. 6402–6413, 2017.

681 Lisa Langnickel, Johannes Darms, Katharina Heldt, Denise Ducks, and Juliane Fluck.
 682 Continuous development of the semantic search engine preVIEW: from COVID-19 to long
 683 COVID. *Database*, 2022, 07 2022. ISSN 1758-0463. doi: 10.1093/database/baac048. URL
 684 <https://doi.org/10.1093/database/baac048>. baac048.

685 Kimin Lee, Kibok Lee, Honglak Lee, and Jinwoo Shin. A simple unified framework for detect-
 686 ing out-of-distribution samples and adversarial attacks. *Advances in neural information
 687 processing systems*, 31, 2018.

688 Weitang Liu, Xiaoyun Wang, John Owens, and Yixuan Li. Energy-based out-of-distribution
 689 detection. In H. Larochelle, M. Ranzato, R. Hadsell, M.F. Balcan, and H. Lin (eds.),
 690 *Advances in Neural Information Processing Systems*, volume 33, pp. 21464–21475. Curran
 691 Associates, Inc., 2020a. URL <https://proceedings.neurips.cc/paper/2020/file/f5496252609c43eb8a3d147ab9b9c006-Paper.pdf>.

692 Weitang Liu, Xiaoyun Wang, John Owens, and Yixuan Li. Energy-based out-of-distribution
 693 detection. *Advances in neural information processing systems*, 33:21464–21475, 2020b.

702 Xixi Liu, Yaroslava Lochman, and Christopher Zach. Gen: Pushing the limits of softmax-
 703 based out-of-distribution detection. In *Proceedings of the IEEE/CVF Conference on*
 704 *Computer Vision and Pattern Recognition*, pp. 23946–23955, 2023.

705 Philipp Liznerski, Lukas Ruff, Robert A Vandermeulen, Billy Joe Franks, Klaus-Robert
 706 Müller, and Marius Kloft. Exposing outlier exposure: What can be learned from few, one,
 707 and zero outlier images. *arXiv preprint arXiv:2205.11474*, 2022.

708 Ilya Loshchilov and Frank Hutter. Sgdr: Stochastic gradient descent with warm restarts.
 709 *arXiv preprint arXiv:1608.03983*, 2016.

710 Ilya Loshchilov and Frank Hutter. Decoupled weight decay regularization. *arXiv preprint*
 711 *arXiv:1711.05101*, 2017.

712 Lefteris Loukas, Manos Fergadiotis, Ion Androutsopoulos, and Prodromos Malakasiotis.
 713 EDGAR-CORPUS: Billions of tokens make the world go round. In *Proceedings of the*
 714 *Third Workshop on Economics and Natural Language Processing*, pp. 13–18, Punta Cana,
 715 Dominican Republic, November 2021. Association for Computational Linguistics. URL
 716 <https://aclanthology.org/2021.econlp-1.2>.

717 Haodong Lu, Dong Gong, Shuo Wang, Jason Xue, Lina Yao, and Kristen Moore. Learning
 718 with mixture of prototypes for out-of-distribution detection. In *The Twelfth International*
 719 *Conference on Learning Representations*, 2024. URL <https://openreview.net/forum?id=uNkKaD3MCs>.

720 Ian Magnusson, Akshita Bhagia, Valentin Hofmann, Luca Soldaini, Ananya Harsh Jha,
 721 Oyvind Tafjord, Dustin Schwenk, Evan Walsh, Yanai Elazar, Kyle Lo, et al. Paloma: A
 722 benchmark for evaluating language model fit. *Advances in Neural Information Processing*
 723 *Systems*, 37:64338–64376, 2024.

724 Andrey Malinin and Mark Gales. Uncertainty estimation in autoregressive structured
 725 prediction. *arXiv preprint arXiv:2002.07650*, 2020.

726 Andrey Malinin, Neil Band, German Chesnokov, Yarin Gal, Mark JF Gales, Alexey Noskov,
 727 Andrey Ploskonosov, Liudmila Prokhorenkova, Ivan Provilkov, Vatsal Raina, et al. Shifts:
 728 A dataset of real distributional shift across multiple large-scale tasks. *arXiv preprint*
 729 *arXiv:2107.07455*, 2021.

730 Oded Maron and Tomás Lozano-Pérez. A framework for multiple-instance learning. *Advances*
 731 *in neural information processing systems*, 10, 1997.

732 Yifei Ming, Ying Fan, and Yixuan Li. POEM: Out-of-distribution detection with posterior
 733 sampling. In Kamalika Chaudhuri, Stefanie Jegelka, Le Song, Csaba Szepesvari, Gang Niu,
 734 and Sivan Sabato (eds.), *Proceedings of the 39th International Conference on Machine*
 735 *Learning*, volume 162 of *Proceedings of Machine Learning Research*, pp. 15650–15665.
 736 PMLR, 17–23 Jul 2022. URL <https://proceedings.mlr.press/v162/ming22a.html>.

737 Yifei Ming, Yiyou Sun, Ousmane Dia, and Yixuan Li. How to exploit hyperspherical
 738 embeddings for out-of-distribution detection? In *The Eleventh International Conference*
 739 *on Learning Representations*, 2023.

740 Maximilian Müller and Matthias Hein. Mahalanobis++: Improving ood detection via feature
 741 normalization. In *Forty-second International Conference on Machine Learning*, 2025.

742 Shashi Narayan, Shay B Cohen, and Mirella Lapata. Don’t give me the details, just the
 743 summary! topic-aware convolutional neural networks for extreme summarization. *arXiv*
 744 *preprint arXiv:1808.08745*, 2018.

745 Tomoya Nishida, Noboru Harada, Daisuke Niizumi, Davide Albertini, Roberto Sannino,
 746 Simone Pradolini, Filippo Augusti, Keisuke Imoto, Kota Dohi, Harsh Purohit, et al.
 747 Description and discussion on dcase 2024 challenge task 2: First-shot unsupervised
 748 anomalous sound detection for machine condition monitoring. *arXiv e-prints*, pp. arXiv–
 749 2406, 2024.

756 Long Ouyang, Jeffrey Wu, Xu Jiang, Diogo Almeida, Carroll Wainwright, Pamela Mishkin,
 757 Chong Zhang, Sandhini Agarwal, Katarina Slama, Alex Ray, et al. Training language
 758 models to follow instructions with human feedback. *Advances in neural information*
 759 *processing systems*, 35:27730–27744, 2022.

760 Fabian Paischer, Thomas Adler, Vihang Patil, Angela Bitto-Nemling, Markus Holzleitner,
 761 Sebastian Lehner, Hamid Eghbal-Zadeh, and Sepp Hochreiter. History compression via
 762 language models in reinforcement learning. In *International Conference on Machine*
 763 *Learning*, pp. 17156–17185. PMLR, 2022.

764 Seongheon Park, Xuefeng Du, Min-Hsuan Yeh, Haobo Wang, and Yixuan Li. Steer llm
 765 latents for hallucination detection. *arXiv preprint arXiv:2503.01917*, 2025.

766 Hezhe Qiao, Qingsong Wen, Xiaoli Li, Ee-Peng Lim, and Guansong Pang. Generative
 767 semi-supervised graph anomaly detection. *Advances in neural information processing*
 768 *systems*, 37:4660–4688, 2024.

769 H. Ramsauer, B. Schäfl, J. Lehner, P. Seidl, M. Widrich, L. Gruber, M. Holzleitner,
 770 M. Pavlović, G. K. Sandve, V. Greiff, D. Kreil, M. Kopp, G. Klambauer, J. Brandstetter,
 771 and S. Hochreiter. Hopfield networks is all you need. In *9th International Conference*
 772 *on Learning Representations (ICLR)*, 2021. URL <https://openreview.net/forum?id=tL89RnzIiCd>.

773 Jie Ren, Jiaming Luo, Yao Zhao, Kundan Krishna, Mohammad Saleh, Balaji Lakshmi-
 774 narayanan, and Peter J Liu. Out-of-distribution detection and selective generation for
 775 conditional language models. In *The Eleventh International Conference on Learning*
 776 *Representations*, 2023. URL <https://openreview.net/forum?id=kJUS5nD0vPB>.

777 Karsten Roth, Latha Pemula, Joaquin Zepeda, Bernhard Schölkopf, Thomas Brox, and
 778 Peter Gehler. Towards total recall in industrial anomaly detection. In *Proceedings of the*
 779 *IEEE/CVF Conference on Computer Vision and Pattern Recognition*, pp. 14318–14328,
 2022.

780 Lukas Ruff, Robert Vandermeulen, Nico Goernitz, Lucas Deecke, Shoaib Ahmed Siddiqui,
 781 Alexander Binder, Emmanuel Müller, and Marius Kloft. Deep one-class classification. In
 782 *International conference on machine learning*, pp. 4393–4402. PMLR, 2018.

783 Lukas Ruff, Robert A Vandermeulen, Nico Görnitz, Alexander Binder, Emmanuel Müller,
 784 Klaus-Robert Müller, and Marius Kloft. Deep semi-supervised anomaly detection. *arXiv*
 785 *preprint arXiv:1906.02694*, 2019.

786 Lukas Ruff, Jacob R Kauffmann, Robert A Vandermeulen, Grégoire Montavon, Wojciech
 787 Samek, Marius Kloft, Thomas G Dietterich, and Klaus-Robert Müller. A unifying review
 788 of deep and shallow anomaly detection. *Proceedings of the IEEE*, 109(5):756–795, 2021.

789 Ana Sanchez-Fernandez, Elisabeth Rumetshofer, Sepp Hochreiter, and Guenter Klambauer.
 790 CLOOME: a new search engine unlocks bioimaging databases for queries with chemical
 791 structures. *bioRxiv*, 2022.

792 Bernhard Schäfl, Lukas Gruber, Angela Bitto-Nemling, and Sepp Hochreiter. Hopular:
 793 Modern Hopfield networks for tabular data. *arXiv preprint arXiv:2206.00664*, 2022.

794 Johannes Schimunek, Philipp Seidl, Lukas Friedrich, Daniel Kuhn, Friedrich Rippmann,
 795 Sepp Hochreiter, and Günter Klambauer. Context-enriched molecule representations
 796 improve few-shot drug discovery. In *The Eleventh International Conference on Learning*
 797 *Representations*, 2023.

798 Bernhard Schölkopf, Robert C Williamson, Alex Smola, John Shawe-Taylor, and John Platt.
 799 Support vector method for novelty detection. *Advances in neural information processing*
 800 *systems*, 12, 1999.

801 Bernhard Schölkopf, John C Platt, John Shawe-Taylor, Alex J Smola, and Robert C
 802 Williamson. Estimating the support of a high-dimensional distribution. *Neural computation*,
 803 13(7):1443–1471, 2001.

810 Abigail See, Peter J Liu, and Christopher D Manning. Get to the point: Summarization
 811 with pointer-generator networks. *arXiv preprint arXiv:1704.04368*, 2017.

812

813 Vikash Sehwag, Mung Chiang, and Prateek Mittal. Ssd: A unified framework for self-
 814 supervised outlier detection. *arXiv preprint arXiv:2103.12051*, 2021.

815

816 Zhuchen Shao, Hao Bian, Yang Chen, Yifeng Wang, Jian Zhang, Xiangyang Ji, et al.
 817 Transmil: Transformer based correlated multiple instance learning for whole slide image
 818 classification. *Advances in neural information processing systems*, 34:2136–2147, 2021.

819

820 Yiyou Sun and Yixuan Li. Dice: Leveraging sparsification for out-of-distribution detection.
 821 In *European Conference on Computer Vision*, pp. 691–708. Springer, 2022.

822

823 Yiyou Sun, Chuan Guo, and Yixuan Li. React: Out-of-distribution detection with rectified
 824 activations. *Advances in Neural Information Processing Systems*, 34:144–157, 2021.

825

826 Yiyou Sun, Yifei Ming, Xiaojin Zhu, and Yixuan Li. Out-of-distribution detection with deep
 827 nearest neighbors. In *International Conference on Machine Learning*, pp. 20827–20840.
 828 PMLR, 2022.

829

830 Leitian Tao, Xuefeng Du, Xiaojin Zhu, and Yixuan Li. Non-parametric outlier synthesis.
 831 *arXiv preprint arXiv:2303.02966*, 2023.

832

833 David MJ Tax and Robert PW Duin. Support vector data description. *Machine learning*, 54
 834 (1):45–66, 2004.

835

836 Jörg Tiedemann. Parallel data, tools and interfaces in opus. In *Lrec*, volume 2012, pp.
 837 2214–2218. Citeseer, 2012.

838

839 A. Vaswani, N. Shazeer, N. Parmar, J. Uszkoreit, L. Jones, A. N. Gomez, L. Kaiser,
 840 and I. Polosukhin. Attention is all you need. In I. Guyon, U. V. Luxburg, S. Bengio,
 841 H. Wallach, R. Fergus, S. Vishwanathan, and R. Garnett (eds.), *Advances in Neural
 842 Information Processing Systems 30*, pp. 5998–6008. Curran Associates, Inc., 2017a.

843

844 Ashish Vaswani, Noam Shazeer, Niki Parmar, Jakob Uszkoreit, Llion Jones, Aidan N Gomez,
 845 Łukasz Kaiser, and Illia Polosukhin. Attention is all you need. *Advances in neural
 846 information processing systems*, 30, 2017b.

847

848 Haoqi Wang, Zhizhong Li, Litong Feng, and Wayne Zhang. Vim: Out-of-distribution with
 849 virtual-logit matching. In *Proceedings of the IEEE/CVF conference on computer vision
 850 and pattern recognition*, pp. 4921–4930, 2022.

851

852 Qizhou Wang, Zhen Fang, Yonggang Zhang, Feng Liu, Yixuan Li, and Bo Han. Learning
 853 to augment distributions for out-of-distribution detection. In *NeurIPS*, 2023. URL
 854 <https://openreview.net/forum?id=0tU6VvXJue>.

855

856 Yiming Wang, Pei Zhang, Baosong Yang, Derek Wong, Zhuosheng Zhang, and Rui Wang. Em-
 857 bedding trajectory for out-of-distribution detection in mathematical reasoning. *Advances
 858 in Neural Information Processing Systems*, 37:42965–42999, 2024.

859

860 Jason Wei, Maarten Bosma, Vincent Zhao, Kelvin Guu, Adams Wei Yu, Brian Lester,
 861 Nan Du, Andrew M. Dai, and Quoc V Le. Finetuned language models are zero-shot
 862 learners. In *International Conference on Learning Representations*, 2022. URL <https://openreview.net/forum?id=gEZrGCozdqR>.

863

864 M. Widrich, B. Schäfl, M. Pavlović, H. Ramsauer, L. Gruber, M. Holzleitner, J. Brandstetter,
 865 G. K. Sandve, V. Greiff, S. Hochreiter, and G. Klambauer. Modern Hopfield networks and
 866 attention for immune repertoire classification. *ArXiv*, 2007.13505, 2020a.

867

868 Michael Widrich, Bernhard Schäfl, Milena Pavlović, Hubert Ramsauer, Lukas Gruber, Markus
 869 Holzleitner, Johannes Brandstetter, Geir Kjetil Sandve, Victor Greiff, Sepp Hochreiter, et al.
 870 Modern hopfield networks and attention for immune repertoire classification. *Advances in
 871 neural information processing systems*, 33:18832–18845, 2020b.

864 Tim Z Xiao, Aidan N Gomez, and Yarin Gal. Wat zei je? detecting out-of-distribution
 865 translations with variational transformers. *arXiv preprint arXiv:2006.08344*, 2020.
 866

867 Kai Xu, Rongyu Chen, Gianni Franchi, and Angela Yao. Scaling for training time and post-
 868 hoc out-of-distribution detection enhancement. In *The Twelfth International Conference
 869 on Learning Representations*, 2024.

870 An Yang, Anfeng Li, Baosong Yang, Beichen Zhang, Binyuan Hui, Bo Zheng, Bowen Yu,
 871 Chang Gao, Chengen Huang, Chenxu Lv, et al. Qwen3 technical report. *arXiv preprint
 872 arXiv:2505.09388*, 2025.

873 Jingkang Yang, Pengyun Wang, Dejian Zou, Zitang Zhou, Kunyuan Ding, Wenxuan Peng,
 874 Haoqi Wang, Guangyao Chen, Bo Li, Yiyou Sun, et al. Openood: Benchmarking generalized
 875 out-of-distribution detection. *Advances in Neural Information Processing Systems*, 35:
 876 32598–32611, 2022.

877 Jinsung Yoon, Kihyuk Sohn, Chun-Liang Li, Sercan O Arik, and Tomas Pfister. Spade:
 878 Semi-supervised anomaly detection under distribution mismatch. *Transactions on Machine
 879 Learning Research*, 2023.

880 Jingqing Zhang, Yao Zhao, Mohammad Saleh, and Peter Liu. Pegasus: Pre-training with
 881 extracted gap-sentences for abstractive summarization. In *International conference on
 882 machine learning*, pp. 11328–11339. PMLR, 2020.

883 Jingyang Zhang, Nathan Inkawich, Randolph Linderman, Yiran Chen, and Hai Li. Mixture
 884 outlier exposure: Towards out-of-distribution detection in fine-grained environments. In
 885 *Proceedings of the IEEE/CVF Winter Conference on Applications of Computer Vision
 886 (WACV)*, pp. 5531–5540, January 2023a.

887 Jinsong Zhang, Qiang Fu, Xu Chen, Lun Du, Zelin Li, Gang Wang, Shi Han, Dongmei Zhang,
 888 et al. Out-of-distribution detection based on in-distribution data patterns memorization
 889 with modern Hopfield energy. In *The Eleventh International Conference on Learning
 890 Representations*, 2023b.

891 Jianing Zhu, Yu Geng, Jiangchao Yao, Tongliang Liu, Gang Niu, Masashi Sugiyama, and
 892 Bo Han. Diversified outlier exposure for out-of-distribution detection via informative
 893 extrapolation. *Advances in Neural Information Processing Systems*, 36, 2023.

894

895

896

897

898

899

900

901

902

903

904

905

906

907

908

909

910

911

912

913

914

915

916

917

918	TABLE OF CONTENTS	
919		
920	A Related Work	19
921		
922		
923	B Theoretical Notes	20
924	B.1 OOD Score Investigation	20
925	B.2 Mahalanobis Decomposition	20
926	B.3 AP-OOD Reduces to Mahalanobis Distance with Mean Pooling for $\beta = 0$	21
927		
928		
929	C Additional Algorithmic Details	22
930	C.1 Mini-Batch Attention Pooling	22
931	C.2 AP-OOD in PyTorch/Einops-like Pseudocode	22
932	C.3 On the Difference Between Heads and Queries	22
933		
934		
935		
936	D Experiments	23
937	D.1 Additional Details for the Toy Experiment	23
938	D.2 Hyperparameter Selection	23
939	D.3 Supervised Experiments on Text Summarization	24
940	D.4 Visualizing AP-OOD’s Attention Maps on the Summarization Task	25
941	D.5 Supervised Experiments on Translation	27
942	D.6 Experiments on Decoder-Only Language Modeling	27
943	D.7 OOD Score Comparison	27
944	D.8 Ablations	27
945	D.9 Performance Measurements	28
946		
947		
948		
949		
950		
951	E The Use of Large Language Models	31
952		
953		
954		
955		
956		
957		
958		
959		
960		
961		
962		
963		
964		
965		
966		
967		
968		
969		
970		
971		

972 A RELATED WORK
973

974 **Continuous modern Hopfield networks.** Modern Hopfield networks (MHNs) are
975 energy-based associative memory networks. They advance conventional Hopfield networks
976 (Hopfield, 1984) by introducing continuous queries and states and a new energy function.
977 MHNs have exponential storage capacity, while retrieval is possible with a one-step update
978 (Ramsauer et al., 2021). The update rule of MHNs coincides with attention as it is used in
979 the Transformer (Vaswani et al., 2017a). Examples for successful applications of MHNs are
980 Widrich et al. (2020a); Fürst et al. (2022); Sanchez-Fernandez et al. (2022); Paischer et al.
981 (2022); Schäfl et al. (2022); Schimunek et al. (2023); Auer et al. (2023) and Hofmann et al.
982 (2024).

983 **Multiple instance learning (MIL).** MIL (Dietterich et al., 1997; Maron & Lozano-
984 Pérez, 1997; Andrews et al., 2002; Ilse et al., 2018) considers a classifier that maps a bag
985 $Z = (z_1, \dots, z_S)$ of instances z_s to a bag-level label $Y \in \{0, 1\}$. MIL also assumes that
986 individual labels $y_s \in \{0, 1\}$ exist for the instances, which remain unknown during training.
987 By assumption, the bag-level label is positive once one of the instance-level labels is positive
988 (and negative if all are instance-level labels negative), i.e., $Y := \max_s y_s$. Recent MIL
989 methods use attention pooling (Ilse et al., 2018; Shao et al., 2021; Al Hajj et al., 2024) and
990 modern Hopfield networks (Widrich et al., 2020b) to pool the features of the instances.
991

992 **One-class classification (OCC).** OCC (Schölkopf et al., 1999) is the problem of learning
993 a decision boundary separating the ID and OOD regions while having access to examples
994 from the ID data set only. One-Class SVM (Schölkopf et al., 2001) learns a maximum margin
995 hyperplane in the feature space that separates the ID data from the origin. Support Vector
996 Data Description (SVDD; Tax & Duin, 2004) learns a hypersphere which encapsulates the ID
997 data. Most closely related to AP-OOD is Deep SVDD (Ruff et al., 2018). Deep SVDD learns
998 an encoder $\psi(\cdot, \mathcal{W}) : \mathbb{R}^D \rightarrow \mathbb{R}^M$ by minimizing the volume of a data-enclosing hypersphere
999 in the output space. Ruff et al. (2019) propose Deep SAD, an extension of Deep SVDD that
1000 makes use of AUX data during training. However, Liznerski et al. (2022) show that the
1001 effectiveness of this extension degrades with increasing dimensionality.
1002
1003
1004
1005
1006
1007
1008
1009
1010
1011
1012
1013
1014
1015
1016
1017
1018
1019
1020
1021
1022
1023
1024
1025

1026 B THEORETICAL NOTES
10271028 B.1 OOD SCORE INVESTIGATION
1029

1030 In the following, we show that

1031
$$\min_{j \in \{1, \dots, M\}} -d_j^2(\phi_{\text{enc}}(\mathbf{x}), \tilde{\mathbf{Z}}) + \log(\|\mathbf{w}_j\|_2^2) < 2 \log(\epsilon) + \log(2\pi) \implies \mathbf{x} \in \mathbb{O}$$

1032

1033 whenever $z_j := \frac{\mathbf{w}_j^T}{\|\mathbf{w}_j\|_2} \tilde{\mathbf{z}}_j$ is normally distributed with probability density function
1034

1035
$$\dot{p}_j(z_j) := \frac{\|\mathbf{w}_j\|_2}{\sqrt{2\pi}} \exp\left(-\frac{1}{2}(\|\mathbf{w}_j\|_2 z_j - \mathbf{w}_j^T \boldsymbol{\mu}_j)^2\right), \quad (16)$$

1036

1037 weight vectors $\mathbf{w}_j \in \mathbb{R}^D$, encoder $\phi_{\text{enc}} : \mathcal{X} \rightarrow \mathcal{Z}$, $\mathcal{Z} = \bigcup_{S \geq 1} \mathbb{R}^{D \times S}$, $\mathbf{Z} \in \mathcal{Z}$, $\tilde{\mathbf{Z}} \in \mathcal{Z}$, $\tilde{\mathbf{z}}_j = \mathbf{Z} \mathbf{p}_j$,
1038 $\boldsymbol{\mu}_j = \tilde{\mathbf{Z}} \tilde{\mathbf{p}}_j$, $\mathbf{p}_j \in \Delta^S$ and $\tilde{\mathbf{p}}_j \in \Delta^{S'}$ with
1039

1040
$$\Delta^S := \{(p_1, \dots, p_S) \in [0, 1]^S \mid \sum_{i=1}^S p_i = 1\}.$$

1041

1042 *Proof.* Note that the ϕ_{enc} -pushforward density $p_{\phi_{\text{enc}}}$ of p_{ID} satisfies
1043

1044
$$p_{\phi_{\text{enc}}}(\mathbf{Z}) := \int_{\mathcal{X}} p_{\text{ID}}(\mathbf{x}) \delta(\phi_{\text{enc}}(\mathbf{x}) = \mathbf{Z}) d\mathbf{x} \geq p_{\text{ID}}(\mathbf{x}).$$

1045

1046 Analogously, we get $\bar{p}_j(\tilde{\mathbf{z}}_j) \geq p_{\phi_{\text{enc}}}(\mathbf{Z})$ for $\tilde{\mathbf{z}}_j = \mathbf{Z} \mathbf{p}_j$ and $\dot{p}_j(z_j) \geq \bar{p}_j(\tilde{\mathbf{z}}_j)$ for $z_j := \frac{\mathbf{w}_j^T}{\|\mathbf{w}_j\|_2} \tilde{\mathbf{z}}_j$.
10471048 That is, for any $j \in \{1, \dots, M\}$, we have that $p_{\text{ID}}(\mathbf{x}) \leq p_{\phi_{\text{enc}}}(\mathbf{Z}) \leq \bar{p}_j(\tilde{\mathbf{z}}_j) \leq \dot{p}_j(z_j)$. As a
1049 consequence, for all $j \in \{1, \dots, M\}$ it holds that $\dot{p}_j(z_j) < \epsilon \implies p_{\text{ID}}(\mathbf{x}) < \epsilon$. Moreover, the
1050 following equivalence holds:
1051

1052
$$\begin{aligned} \dot{p}_j(z_j) &< \epsilon & \iff \\ \frac{\|\mathbf{w}_j\|_2}{\sqrt{2\pi}} \exp\left(-\frac{1}{2}(\|\mathbf{w}_j\|_2 z_j - \mathbf{w}_j^T \boldsymbol{\mu}_j)^2\right) &< \epsilon & \iff \\ \frac{\|\mathbf{w}_j\|_2}{\sqrt{2\pi}} \exp\left(-\frac{1}{2}(\mathbf{w}_j^T \tilde{\mathbf{z}}_j - \mathbf{w}_j^T \boldsymbol{\mu}_j)^2\right) &< \epsilon & \iff \\ -(\mathbf{w}_j^T \tilde{\mathbf{z}}_j - \mathbf{w}_j^T \boldsymbol{\mu}_j)^2 + \log(\|\mathbf{w}_j\|_2^2) &< 2 \log(\epsilon) + \log(2\pi) & (17) \end{aligned}$$

1053

1054 As a consequence, we have that $\mathbf{x} \in \mathbb{O}$, if Equation (17) is satisfied for any $j \in \{1, \dots, M\}$. \square
10551056 B.2 MAHALANOBIS DECOMPOSITION
10571058 We assume the D weight vectors \mathbf{w}_j are linearly independent. First, we start from the
1059 directional decomposition and show the relation to the Mahalanobis distance.
1060

1061
$$d_{\text{Maha}}^2(\tilde{\mathbf{z}}, \boldsymbol{\mu}) = \sum_{j=1}^D (\mathbf{w}_j^T \tilde{\mathbf{z}} - \mathbf{w}_j^T \boldsymbol{\mu})^2 \quad (18)$$

1062

1063
$$= (\tilde{\mathbf{z}} - \boldsymbol{\mu})^T \left(\sum_{i=1}^D \mathbf{w}_i \mathbf{w}_i^T \right) (\tilde{\mathbf{z}} - \boldsymbol{\mu}) \quad (19)$$

1064

1065
$$= (\tilde{\mathbf{z}} - \boldsymbol{\mu})^T \boldsymbol{\Sigma}^{-1} (\tilde{\mathbf{z}} - \boldsymbol{\mu}). \quad (20)$$

1066

1067 Because the weight vectors are linearly independent, $\boldsymbol{\Sigma}^{-1}$ has full rank. Next, we go in
1068 the opposite direction and show that the eigenvectors $\mathbf{V} = (\mathbf{v}_1, \dots, \mathbf{v}_D)$ and eigenvalues
1069 $\mathbf{D} = \text{diag}(\lambda_1, \dots, \lambda_D)$ of a $\boldsymbol{\Sigma}$ can be used to define corresponding \mathbf{w}_j .
1070

1080
1081
1082 $d_{\text{Maha}}^2(\bar{\mathbf{z}}, \boldsymbol{\mu}) = (\bar{\mathbf{z}} - \boldsymbol{\mu})^T \boldsymbol{\Sigma}^{-1}(\bar{\mathbf{z}} - \boldsymbol{\mu}) \quad (21)$
1083 $= (\bar{\mathbf{z}} - \boldsymbol{\mu})^T \mathbf{V}^T \mathbf{D}^{-1} \mathbf{V}(\bar{\mathbf{z}} - \boldsymbol{\mu}) \quad (22)$
1084 $= \left(\sqrt{\mathbf{D}^{-1} \mathbf{V} \bar{\mathbf{z}}} - \sqrt{\mathbf{D}^{-1} \mathbf{V} \boldsymbol{\mu}} \right)^T \left(\sqrt{\mathbf{D}^{-1} \mathbf{V} \bar{\mathbf{z}}} - \sqrt{\mathbf{D}^{-1} \mathbf{V} \boldsymbol{\mu}} \right) \quad (23)$
1085
1086 $= \sum_{j=1}^D (\mathbf{w}_j^T \bar{\mathbf{z}} - \mathbf{w}_j^T \boldsymbol{\mu})^2, \quad (24)$
1087
1088
1089

1090 where $\mathbf{w}_j = \sqrt{\lambda_j^{-1}} \mathbf{v}_j$, $\boldsymbol{\Sigma} = \mathbf{V}^T \mathbf{D} \mathbf{V}$, and $\boldsymbol{\Sigma}^{-1} = \mathbf{V}^T \mathbf{D}^{-1} \mathbf{V}$.

1091 The relation between the Mahalanobis distance and the directional decomposition is as
1092 follows:

1093 1. Any linearly independent sequence $\mathbf{w}_1, \dots, \mathbf{w}_D$ induces a positive definite matrix $\boldsymbol{\Sigma}^{-1} :=$
1094 $\sum_{j=1}^D \mathbf{w}_j \mathbf{w}_j^\top$, and hence a Mahalanobis distance satisfying

1095
1096
1097 $\sum_{j=1}^D (\mathbf{w}_j^\top \bar{\mathbf{z}} - \mathbf{w}_j^\top \boldsymbol{\mu})^2 = (\bar{\mathbf{z}} - \boldsymbol{\mu})^T \boldsymbol{\Sigma}^{-1}(\bar{\mathbf{z}} - \boldsymbol{\mu}). \quad (25)$
1098
1099
1100

1101 2. Conversely, any full-rank covariance matrix $\boldsymbol{\Sigma}$ admits a set of linearly independent vectors
1102 $\mathbf{w}_1, \dots, \mathbf{w}_D$ such that $\boldsymbol{\Sigma}^{-1} = \sum_{j=1}^D \mathbf{w}_j \mathbf{w}_j^\top$, and therefore Equation (25) holds.

1103 Thus, our decomposition and the Mahalanobis form represent the same quadratic form; the
1104 eigen-decomposition is only one possible choice of \mathbf{w}_j .

1105 B.3 AP-OOD REDUCES TO MAHALANOBIS DISTANCE WITH MEAN POOLING FOR $\beta = 0$

1106 In this section, we show that as $\beta = 0$ and $M = D$, $d^2(\mathbf{Z}, \tilde{\mathbf{Z}})$ reduces to the Mahalanobis
1107 distance with mean pooling as used by Ren et al. (2023). To arrive at the result, we assume
1108 uniform sequence lengths.

1109
1110 $\text{softmax}(0 \cdot \mathbf{Z}^T \mathbf{w})_s = \frac{\exp(0 \cdot \mathbf{z}_s^T \mathbf{w})}{\sum_{s'=1}^S \exp(0 \cdot \mathbf{z}_{s'}^T \mathbf{w})} = \frac{1}{S}, \quad (26)$
1111
1112
1113

1114
1115 $\bar{\mathbf{z}} = \text{AttPool}_0(\mathbf{Z}, \mathbf{w}) = \mathbf{Z} \text{softmax}(0 \cdot \mathbf{Z}^T \mathbf{w}) = \frac{1}{S} \sum_{s=1}^S \mathbf{z}_s, \quad (27)$
1116
1117
1118

1119
1120 $\boldsymbol{\mu} = \text{AttPool}_0(\tilde{\mathbf{Z}}, \mathbf{w}) = \tilde{\mathbf{Z}} \text{softmax}(0 \cdot \tilde{\mathbf{Z}}^T \mathbf{w}) = \frac{1}{SN} \sum_{i=1}^N \sum_{s=1}^S \mathbf{z}_{is} = \frac{1}{N} \sum_{i=1}^N \bar{\mathbf{z}}_i, \quad (28)$
1121
1122

1123 where we use the concatenated sequence $\tilde{\mathbf{Z}} = (\mathbf{Z}_1 \| \dots \| \mathbf{Z}_N)$, and the sequence representations
1124 $\mathbf{Z}_i = \phi(\mathbf{x}_i) = (\mathbf{z}_{i1}, \dots, \mathbf{z}_{iS}) \in \mathbb{R}^{D \times S}$. The squared distance of AP-OOD reduces to

1125
1126 $d^2(\mathbf{Z}, \tilde{\mathbf{Z}}) = \sum_{j=1}^M \left(\mathbf{w}_j^T \mathbf{Z} \text{softmax}(\beta \mathbf{Z}^T \mathbf{w}_j) - \mathbf{w}_j^T \tilde{\mathbf{Z}} \text{softmax}(\beta \tilde{\mathbf{Z}}^T \mathbf{w}_j) \right)^2 \quad (29)$
1127
1128

1129
1130 $= \sum_{j=1}^D (\mathbf{w}_j^T \bar{\mathbf{z}} - \mathbf{w}_j^T \boldsymbol{\mu})^2 = d_{\text{Maha}}^2(\bar{\mathbf{z}}, \boldsymbol{\mu}). \quad (30)$
1131
1132
1133

1134 C ADDITIONAL ALGORITHMIC DETAILS
11351136 C.1 MINI-BATCH ATTENTION POOLING
11371138 In this section, we describe the process of performing attention pooling over a long sequence
1139 $\tilde{\mathbf{Z}}$ that is too large to fit into memory by dividing $\tilde{\mathbf{Z}}$ into smaller mini-batches **of size**
1140 $B \in \mathbb{N}$. For this, we need the log-sum-exponential (lse) function. We follow the notation
1141 from [Ramsauer et al. \(2021\)](#):

1142
1143
$$\text{lse}(\beta, \mathbf{a}) = \beta^{-1} \log \left(\sum_{s=1}^S \exp(\beta a_s) \right) \quad (31)$$

1144

1145 The following algorithm computes $\mu = \tilde{\mathbf{Z}} \text{softmax}(\beta \tilde{\mathbf{Z}}^T \mathbf{w})$ for $\beta > 0$:
11461147
1148 **Algorithm 2** Attention pooling over a long sequence1149 **Require:** $\tilde{\mathbf{Z}} = (\tilde{\mathbf{z}}_1, \dots, \tilde{\mathbf{z}}_S) \in \mathbb{R}^{D \times S}$, inverse temperature β , weight vector \mathbf{w} , batch size B
1150 1: $E \leftarrow -\infty$
1151 2: $\mu \leftarrow \mathbf{0}$
1152 3: **for** $s \leftarrow 1$ to S **step** B **do**
1153 4: Load mini-batch $\mathbf{B} \leftarrow (\tilde{\mathbf{z}}_s, \dots, \tilde{\mathbf{z}}_{s+B})$
1154 5: $E_B \leftarrow \text{lse}(\beta, \mathbf{B}^T \mathbf{w})$
1155 6: $\mathbf{p} \leftarrow \exp(\beta(\mathbf{B}^T \mathbf{w} - E_B))$
1156 7: $\mu_B \leftarrow \mathbf{B} \mathbf{p}$
1157 8: $p_B \leftarrow \sigma(\beta(E_B - E))$
1158 9: $\mu \leftarrow p_B \mu_B + (1 - p_B) \mu$
1159 10: $E \leftarrow \beta^{-1} \log(\exp(\beta E_B) + \exp(\beta E))$
1160 **return** μ 1161
1162 C.2 AP-OOD IN PyTorch/Einops-LIKE PSEUDOCODE
11631164 We detail the loss computation for AP-OOD with multiple queries per head (Equation (14))
1165 using PyTorch/Einops-style pseudocode. Assuming a uniform sequence length S , Algorithm
1166 3 demonstrates the computation via attention pooling over the sequences \mathbf{Z} . Alternatively,
1167 Algorithm 4 presents a mathematically equivalent formulation that applies attention pooling
1168 over the similarities $\mathbf{W}^T \mathbf{Z}$.
11691170 C.3 ON THE DIFFERENCE BETWEEN HEADS AND QUERIES
11711172 We find that heads are learnt largely independently from one another while queries are not,
1173 which we experimentally verify as follows: We train AP-OOD using the SGD optimizer on
1174 the summarization task using (i) 1 head and (ii) 2 heads, where the initialization of one
1175 of the heads in (ii) is identical to the initialization of the head of (i). We find that after
1176 training for 500 steps, the weight vectors associated with the heads with shared initialization
1177 between (i) and (ii) remain identical. In contrast, when repeating this experiment by varying
1178 the number of queries, the weight vectors associated with the queries differ after training.
1179 Intuitively, adding additional heads will help the model discover more local minima in the
1180 parameter space (similar to [Lakshminarayanan et al., 2017](#)), while adding queries increases
1181 the capacity of each given head. The following observation supports this intuition: When
1182 testing different hyperparameter combinations for AP-OOD, we found that a large number
1183 of queries combined with a small number of heads leads to overfitting when training the
1184 model on small ID data sets (e.g., 10,000 sequences): In this case, the average distance of the
1185 ID training sequences is substantially smaller than the average distance of the ID validation
1186 sequences.
1187

1188 **Algorithm 3** AP-OOD loss in PyTorch/Einops-like style using attention pooling over \mathbf{Z}

```

1189
1190 1  def attention_pooling(Zs, Ws):
1191 2      # Zs[N S D] - mini-batch of N sequences with length S
1192 3      # Ws[M T D] - weights of model with M heads and T queries
1193 4
1194 5      # pairwise similarities between tokens and weights
1195 6      similarities = einsum(Zs, Ws, 'N S D, M T D -> N M S T')
1196 7
1197 8      # softmax over query- and sequence dimensions
1198 9      probs = similarities.softmax(dim=(-2, -1)) #[N M S T]
119910
120011      # pooling to form new sequences
120112      Z_bars = einsum(Zs, probs, 'N S D, N M S T -> N M T D')
120213
120314      return Z_bars
120415
120516  def loss(Zs, Ws):
120617      # Zs[N S D] - mini-batch of N sequences with length S
120718      # Ws[M T D] - weights of model with M heads and T queries
120819
120920      # attention pooling over individual sequence
121021      Z_bars = attention_pooling(Zs, Ws) #[N M T D]
121122
121223      # attention pooling over all sequences
121324      Z_tilde = Zs.flatten(0, 1).unsqueeze(0) #[1, N*S, D]
121425      mus = attention_pooling(Z_tilde, Ws) #[1 M T D]
121526
121627      # squared distance per head
121728      heads_Z = einsum(Z_bars, Ws, 'N M T D, M T D -> N M')
121829      heads_mu = einsum(mus, Ws, '1 M T D, M T D -> 1 M')
121930      ds_squared = (heads_Z - heads_mu)**2 #[N M]
122031
122132      # regularized and loss
122233      regularizer = torch.log((Ws * Ws).sum(1, 2)) #[M]
122334      losses = torch.sum(ds_squared - regularizer, dim=1) #[N]
122435      loss = torch.mean(losses)
122536
122637      return loss
1227
1228
1229
```

D EXPERIMENTS

D.1 ADDITIONAL DETAILS FOR THE TOY EXPERIMENT

In the toy experiment in Figure 2, we modify the attention pooling process to use the negative squared Euclidean distance instead of the dot product similarity because the Euclidean distance is known to work better in low-dimensional spaces. Formally, the modified attention pooling process is:

$$\text{AttPool}_\beta(\mathbf{Z}, \mathbf{w}) := \sum_{s=1}^S \mathbf{z}_s \frac{\exp(-\frac{\beta}{2} \|\mathbf{z}_s - \mathbf{w}\|_2^2)}{\sum_{s'=1}^S \exp(-\frac{\beta}{2} \|\mathbf{z}_{s'} - \mathbf{w}\|_2^2)}. \quad (32)$$

D.2 HYPERPARAMETER SELECTION

To find the values for β , M , and T in the unsupervised setting, we perform a grid search using the values $\beta \in \{\frac{1}{\sqrt{D}}, 0.25, 0.5, 1, 2\}$ and $T \in \{1, 4, 16\}$. We select M such that the total number of parameters of AP-OOD equals the number of entries in Σ of the Mahalanobis

1242 **Algorithm 4** AP-OOD loss in PyTorch/Einops-like style using attention pooling over $\mathbf{W}^T \mathbf{Z}$

```

1243
1244 1  def attention_pooling(Zs, Ws):
1245 2      # Zs[N S D] - mini-batch of N sequences with length S
1246 3      # Ws[M T D] - weights of model with M heads and T queries
1247 4
1248 5          # pairwise similarities between tokens and weights
1249 6          similarities = einsum(Zs, Ws, 'N S D, M T D -> N M S T')
1250 7
1251 8          # softmax over query- and sequence dimensions
1252 9          probs = similarities.softmax(dim=(-2, -1)) #[N M S T]
125310
125411      # pooling over similarities
125512      pooled = einsum(similarities, probs 'N M S T, N M S T -> N M')
125613
125714      return pooled
125815
125916  def loss(Zs, Ws):
126017      # Zs[N S D] - mini-batch of N sequences with length S
126118      # Ws[M T D] - weights of model with M heads and T queries
126219
126320      # attention pooling over individual sequence
126421      heads_Z = attention_pooling(Zs, Ws) #[N M]
126522
126623      # attention pooling over all sequences
126724      Z_tilde = Zs.flatten(0, 1).unsqueeze(0) #[1, N*S, D]
126825      heads_mu = attention_pooling(Z_tilde, Ws) #[1 M]
126926
127027      # squared distance per head
127128      ds_squared = (heads_Z - heads_mu)**2 #[N M]
127229
127330      # regularizer and loss
127431      regularizer = torch.log((Ws * Ws).sum(1, 2)) #[M]
127532      losses = torch.sum(ds_squared - regularizer, dim=1) #[N]
127633      loss = torch.mean(losses)
127734
127835      return loss

```

1278 method, i.e., such that $MT = D$. We select the hyperparameter configuration by evaluating
1279 each resulting model on OOD detection using a validation split of the AUX data set (in the
1280 unsupervised setting, we use the AUX data set only for model selection, not for training the
1281 model), and we select the model with the highest AUROC. In the supervised setting, we
1282 follow the same procedure, and we additionally select $\lambda \in \{0.1, 1, 10\}$.

1284

1285 D.3 SUPERVISED EXPERIMENTS ON TEXT SUMMARIZATION

1286 In the fully supervised setting, we train all methods on the embeddings of 100,000 ID examples
1287 and 10,000 AUX examples obtained from PEGASUS_{LARGE} trained on text summarization
1288 using the XSUM data set. Table 4 shows that AP-OOD substantially improves fully
1289 supervised OOD detection results, improving the previously best mean FPR95 of 1.06%
1290 (binary logits) to 0.28% in the input OOD setting. Figure 5 shows the results for the
1291 semi-supervised setting when scaling the number of AUX examples on all OOD data sets for
1292 text summarization. We evaluate relative Mahalanobis only for $N' \geq 1024$, because Σ is not
1293 invertible when using fewer AUX examples. In contrast to Figure 3, Figure 5 also shows the
1294 results for Reddit TIFU and Samsum. On these two data sets, all evaluated methods except
1295 relative Mahalanobis achieve near-perfect OOD detection results for $N' \geq 8$.

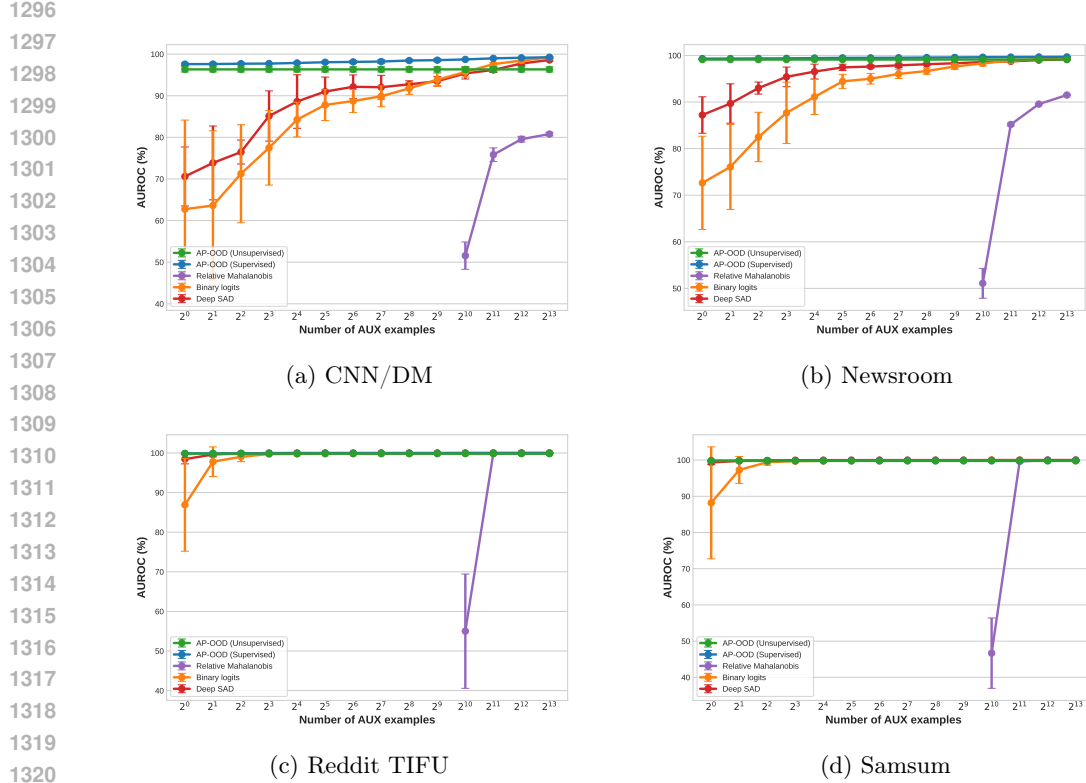


Figure 5: OOD detection performance on text summarization for all OOD data sets. We vary the number of AUX examples and compare results from AP-OOD, binary logits (Ren et al., 2023), relative Mahalanobis (Ren et al., 2023), and Deep SAD (Ruff et al., 2019).

Table 4: Supervised OOD detection performance on text summarization. We compare results from AP-OOD, binary logits (Ren et al., 2023), relative Mahalanobis (Ren et al., 2023), and Deep SAD (Ruff et al., 2019) on PEGASUS_{LARGE} trained on XSUM as the ID data set. ↓ indicates “lower is better” and ↑ “higher is better”. All values in %. We estimate standard deviations across five independent data set splits and training runs.

		CNN/DM	Newsroom	Reddit	Samsum	Mean
	Input OOD					
Binary logits	AUROC ↑ FPR95 ↓	99.43 ± 0.11 2.32 ± 0.59	99.52 ± 0.06 1.93 ± 0.17	100.00 ± 0.00 0.00 ± 0.00	99.99 ± 0.00 0.01 ± 0.01	99.73 1.06
Relative Mahalanobis	AUROC ↑ FPR95 ↓	81.28 ± 0.19 62.92 ± 0.34	91.85 ± 0.20 28.22 ± 0.43	99.96 ± 0.00 0.00 ± 0.01	99.98 ± 0.00 0.01 ± 0.01	93.27 22.79
Deep SAD	AUROC ↑ FPR95 ↓	98.85 ± 0.17 3.69 ± 0.81	99.24 ± 0.07 2.38 ± 0.16	100.00 ± 0.00 0.00 ± 0.00	100.00 ± 0.00 0.00 ± 0.00	99.52 1.52
AP-OOD (Ours)	AUROC ↑ FPR95 ↓	99.83 ± 0.18 0.37 ± 0.51	99.71 ± 0.05 0.76 ± 0.19	100.00 ± 0.00 0.00 ± 0.00	100.00 ± 0.00 0.00 ± 0.00	99.88 0.28
	Output OOD					
Binary logits	AUROC ↑ FPR95 ↓	98.67 ± 0.26 5.01 ± 0.97	99.49 ± 0.03 1.77 ± 0.07	99.99 ± 0.01 0.00 ± 0.00	99.94 ± 0.02 0.09 ± 0.04	99.52 1.72
Relative Mahalanobis	AUROC ↑ FPR95 ↓	93.58 ± 0.18 24.32 ± 0.33	97.41 ± 0.08 8.54 ± 0.23	99.82 ± 0.01 0.04 ± 0.01	99.54 ± 0.03 1.00 ± 0.09	97.59 8.47
Deep SAD	AUROC ↑ FPR95 ↓	98.39 ± 0.23 6.00 ± 0.75	99.53 ± 0.03 1.66 ± 0.14	100.00 ± 0.00 0.00 ± 0.00	99.96 ± 0.00 0.07 ± 0.03	99.47 1.93
AP-OOD (Ours)	AUROC ↑ FPR95 ↓	99.00 ± 0.13 3.25 ± 0.42	99.59 ± 0.02 1.24 ± 0.07	100.00 ± 0.00 0.00 ± 0.00	99.98 ± 0.00 0.01 ± 0.01	99.64 1.13

D.4 VISUALIZING AP-OOD’s ATTENTION MAPS ON THE SUMMARIZATION TASK

We analyze how the attention pooling process of AP-OOD allocates weight to individual tokens. We randomly select one sample from each of the four OOD data sets in the

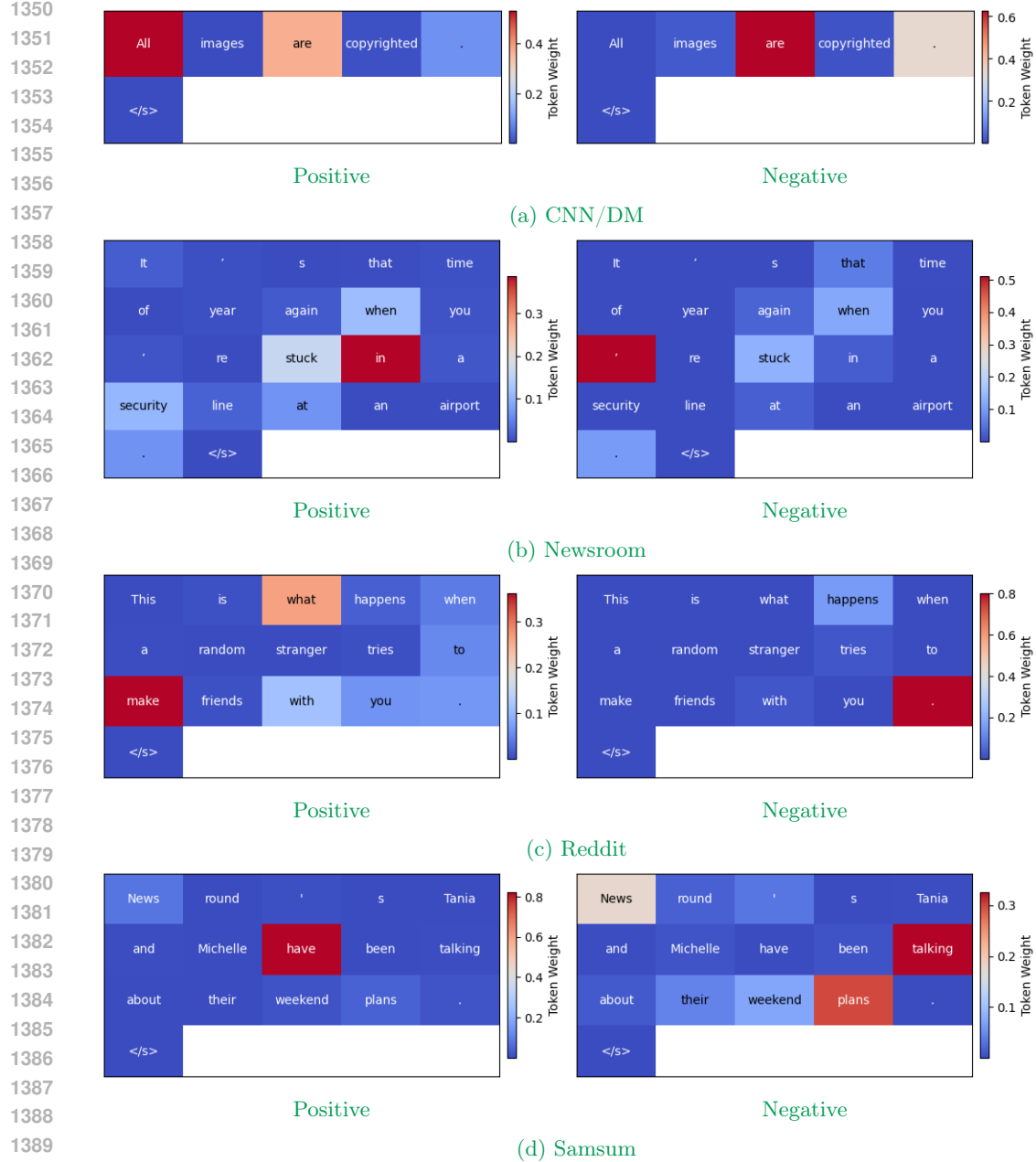


Figure 6: AP-OOD’s attention weights on randomly selected output sequences from OOD data sets on text summarization. For each sequence, we visualize the heads j with the highest deviation in the positive and negative direction of the $d_j(\mathbf{Z})$ before applying the square.

summarization benchmark. We then investigate the attention weights of a trained AP-OOD model over the generated output sequence. For each sample, we select the two heads with the largest deviations in the positive and in the negative directions before applying the square in the score function of AP-OOD. Figure 6 visualizes the token-wise attention scores of the selected heads. When manually examining the generated output sequences, we find it hard to attribute the “OODness” of individual sequences to a single token or to a small set of tokens. Therefore, it is difficult to interpret the attention scores for the individual heads. However, the results indicate that the different heads exhibit distinct attention patterns.

1404

1405 Table 5: Supervised OOD detection performance on English-to-French translation. We
 1406 compare results from AP-OOD, binary logits, relative mahalanobis (Ren et al., 2023), and
 1407 Deep SAD (Ruff et al., 2019) on a Transformer (base) trained on WMT15 En–Fr as the ID
 1408 data set. \downarrow indicates “lower is better” and \uparrow “higher is better”. All values in %. We estimate
 1409 standard deviations across five independent data set splits and training runs.

1410

1411

	IT	Koran	Law	Medical	Subtitles	ndd2015	ndt2015	nt2014	Mean
Input OOD									
Binary logits	AUROC \uparrow	93.60 \pm 0.34	95.17 \pm 0.05	54.29 \pm 0.33	70.47 \pm 0.67	90.53 \pm 0.46	89.91 \pm 0.15	89.80 \pm 0.16	85.65 \pm 0.06
	FPR95 \downarrow	28.58 \pm 1.19	34.91 \pm 0.75	97.16 \pm 0.06	82.27 \pm 0.64	41.03 \pm 0.96	60.64 \pm 0.41	57.56 \pm 0.58	75.78 \pm 0.44
Relative Mahalanobis	AUROC \uparrow	92.82 \pm 0.26	93.31 \pm 0.09	43.07 \pm 0.38	74.40 \pm 0.40	95.73 \pm 0.21	89.35 \pm 0.04	88.88 \pm 0.05	82.06 \pm 0.13
	FPR95 \downarrow	19.27 \pm 0.44	53.50 \pm 0.68	94.27 \pm 0.24	67.63 \pm 0.66	13.38 \pm 0.28	59.06 \pm 0.43	61.49 \pm 0.37	83.24 \pm 0.14
Deep SAD	AUROC \uparrow	94.56 \pm 0.13	94.77 \pm 0.14	57.44 \pm 0.58	71.67 \pm 0.27	91.57 \pm 0.21	90.07 \pm 0.16	89.47 \pm 0.12	84.42 \pm 0.19
	FPR95 \downarrow	28.31 \pm 0.62	40.77 \pm 1.35	97.10 \pm 0.13	83.74 \pm 0.28	41.15 \pm 1.24	61.54 \pm 0.81	62.11 \pm 0.82	79.33 \pm 0.65
AP-OOD (Ours)	AUROC \uparrow	94.97 \pm 0.54	96.17 \pm 0.35	56.82 \pm 1.03	79.31 \pm 0.99	95.03 \pm 0.41	90.66 \pm 0.39	90.73 \pm 0.36	86.56 \pm 0.36
	FPR95 \downarrow	29.93 \pm 2.86	26.04 \pm 2.97	94.46 \pm 0.83	79.06 \pm 1.44	29.17 \pm 2.32	56.34 \pm 2.46	55.12 \pm 1.47	69.75 \pm 1.36
Output OOD									
Binary logits	AUROC \uparrow	95.15 \pm 0.06	95.64 \pm 0.17	58.96 \pm 0.79	74.70 \pm 0.37	92.79 \pm 0.22	90.32 \pm 0.19	90.21 \pm 0.16	85.73 \pm 0.12
	FPR95 \downarrow	27.58 \pm 0.44	30.49 \pm 1.89	96.36 \pm 0.28	82.09 \pm 0.61	39.08 \pm 1.07	57.36 \pm 0.98	57.65 \pm 0.68	75.34 \pm 0.41
Relative Mahalanobis	AUROC \uparrow	92.83 \pm 0.18	94.94 \pm 0.14	41.88 \pm 0.42	71.09 \pm 0.27	95.14 \pm 0.16	88.86 \pm 0.02	87.83 \pm 0.08	82.59 \pm 0.10
	FPR95 \downarrow	28.72 \pm 0.40	36.30 \pm 1.18	95.54 \pm 0.29	80.88 \pm 0.20	20.42 \pm 0.57	67.39 \pm 0.52	67.80 \pm 0.48	85.74 \pm 0.20
Deep SAD	AUROC \uparrow	95.88 \pm 0.13	96.57 \pm 0.21	56.47 \pm 1.31	76.35 \pm 0.60	94.79 \pm 0.12	90.66 \pm 0.11	90.40 \pm 0.11	86.21 \pm 0.18
	FPR95 \downarrow	23.73 \pm 0.47	21.38 \pm 1.75	95.86 \pm 0.38	82.47 \pm 0.52	30.23 \pm 0.82	58.14 \pm 1.45	57.37 \pm 1.64	75.73 \pm 0.23
AP-OOD (Ours)	AUROC \uparrow	95.82 \pm 0.24	96.85 \pm 0.24	59.22 \pm 0.92	78.27 \pm 1.67	95.78 \pm 0.13	90.31 \pm 0.33	89.87 \pm 0.35	83.97 \pm 0.90
	FPR95 \downarrow	28.51 \pm 1.44	19.94 \pm 1.78	93.65 \pm 0.36	81.37 \pm 0.56	26.96 \pm 1.04	59.28 \pm 1.36	57.48 \pm 1.09	73.64 \pm 1.21

1423

1424

1425 D.5 SUPERVISED EXPERIMENTS ON TRANSLATION

1426

1427 In the fully supervised setting, we train all methods on the embeddings of 100,000 ID
 1428 embeddings and 100,000 AUX embeddings obtained from a Transformer (base) trained
 1429 on WMT15 En–Fr translation. Table 5 shows that AP-OOD improves supervised OOD
 1430 detection results w.r.t. the mean AUROC and mean FPR95 metrics.

1431

1432 D.6 EXPERIMENTS ON DECODER-ONLY LANGUAGE MODELING

1433

1434 To verify the effectiveness of AP-OOD on the decoder-only language modeling paradigm used
 1435 by LLMs, we conduct experiments on Pythia-160M (Biderman et al., 2023), a decoder-only
 1436 language model trained on the Pile (Gao et al., 2020). We evaluate the discriminative
 1437 power of AP-OOD trained in an unsupervised fashion on the 4Chan and Twitter subsets
 1438 of Paloma (Magnusson et al., 2024), the EDGAR annual reports corpus (annual reports of
 1439 public companies between 1993–2020; Loukas et al., 2021), Long-COVID related articles
 1440 (Langnickel et al., 2022), and the MIMIC-III clinical corpus (Goldberger et al., 2000). In
 1441 the decoder-only setting, we directly use the encoded representations of the input sequences
 1442 and do not generate output sequences. Table 6 shows that AP-OOD improves unsupervised
 1443 OOD detection w.r.t. the mean AUROC and mean FPR95 metrics.

1444

1445 D.7 OOD SCORE COMPARISON

1446

1447 We experimentally compare the min-based OOD score $s_{\min}(\mathbf{Z})$ and its upper bound $s(\mathbf{Z})$.
 1448 For training, we use the loss from Equation (10) in both settings. The results in Table 7
 1449 show that $s(\mathbf{Z})$ achieves better OOD discrimination w.r.t. the mean AUROC and FPR95.
 1450 While $s_{\min}(\mathbf{Z})$ roughly matches the OOD detection metrics of $s(\mathbf{Z})$ on CNN/DM for both
 1451 input and output, $s_{\min}(\mathbf{Z})$ lags behind $s(\mathbf{Z})$ on the other OOD data sets.

1452

1453 D.8 ABLATIONS

1454

1455 **Beta sensitivity analysis.** We evaluate AP-OOD when varying the hyperparameter β
 1456 on the summarization task. We select β from $\{0, 1/\sqrt{D}, 0.25, 0.5, 1, 2\}$, and we leave the
 1457 settings for M and T unchanged (i.e., they are identical to the settings used in Table 1).
 1458 Table 8 shows that AP-OOD on text summarization is relatively insensitive to the selection
 1459 of β inside the range $[0.25, 2]$ in the input and output settings.

1458
 1459 **Table 6:** Unsupervised OOD detection performance on large-scale language modeling. We
 1460 compare results from AP-OOD, Mahalanobis (Lee et al., 2018; Ren et al., 2023), KNN (Sun
 1461 et al., 2022), DeepSVDD (Ruff et al., 2018), and model perplexity (Ren et al., 2023) on
 1462 Pythia-160M trained on the Pile as the ID data set. \downarrow indicates “lower is better” and \uparrow
 1463 “higher is better”. All values in %. Standard deviations are estimated across five independent
 1464 training runs.

1465

1466

		4Chan	Reports	Covid	Clinical	Twitter	Mean
Input OOD							
Perplexity	AUROC \uparrow	65.05	48.32	89.51	85.86	99.22	77.59
	FPR95 \downarrow	72.66	86.91	68.60	65.22	2.85	59.25
Mahalanobis	AUROC \uparrow	35.27	54.72	75.50	75.67	97.86	67.81
	FPR95 \downarrow	92.93	87.77	98.07	90.79	10.91	76.09
KNN	AUROC \uparrow	39.31	59.41	70.62	75.56	81.50	65.28
	FPR95 \downarrow	98.85	93.26	99.03	95.85	61.12	89.62
Deep SVDD	AUROC \uparrow	55.59	64.06	72.54	73.44	81.08	69.34
	FPR95 \downarrow	88.15	88.94	99.52	96.35	76.72	89.93
AP-OOD (Ours)	AUROC \uparrow	87.97	68.09	91.79	86.44	99.08	86.67
	FPR95 \downarrow	88.34	91.47	40.34	57.38	1.52	55.81

1475

1476

1477 **Table 7:** Unsupervised OOD detection performance on text summarization. We compare
 1478 results from AP-OOD when using $s(\mathbf{Z})$ and $s_{\min}(\mathbf{Z})$, on PEGASUS_{LARGE} trained on XSUM
 1479 as the ID data set. \downarrow indicates “lower is better” and \uparrow “higher is better”. All values in %. We
 1480 estimate standard deviations across five independent dataset splits and training runs.

1481

1482

		CNN/DM	Newsroom	Reddit	Samsum	Mean
Input OOD						
$s(\mathbf{Z})$	AUROC \uparrow	96.13\pm0.44	99.10\pm0.08	99.91\pm0.03	99.80\pm0.04	98.74
	FPR95 \downarrow	19.51 \pm 2.24	4.11\pm0.28	0.00\pm0.01	0.04\pm0.03	5.91
$s_{\min}(\mathbf{Z})$	AUROC \uparrow	96.08 \pm 0.37	97.48 \pm 0.28	99.71 \pm 0.20	97.67 \pm 0.35	97.74
	FPR95 \downarrow	18.78\pm2.73	11.16 \pm 1.21	0.01 \pm 0.01	12.04 \pm 3.04	10.50
Output OOD						
$s(\mathbf{Z})$	AUROC \uparrow	93.37 \pm 0.54	92.62\pm0.67	98.04\pm0.28	98.30\pm0.11	95.59
	FPR95 \downarrow	23.12\pm1.97	29.91\pm2.93	6.34\pm1.56	6.83\pm0.64	16.55
$s_{\min}(\mathbf{Z})$	AUROC \uparrow	93.82\pm1.56	88.30 \pm 3.45	95.94 \pm 2.25	90.13 \pm 4.31	92.05
	FPR95 \downarrow	26.60 \pm 5.53	38.26 \pm 3.73	18.49 \pm 9.01	36.71 \pm 12.40	30.02

1491

1492

1493 **Number of heads M and queries T .** We ablate on the number of heads M and the
 1494 number of queries T of AP-OOD on the summarization task. For this ablation, we select
 1495 $T \in \{1, 2, 4, 8, 16, 32, 64, 128, 512, 1024\}$ and we then select M such that the total number
 1496 of parameters of AP-OOD equals the number of entries in Σ of the Mahalanobis method,
 1497 i.e., such that $MT = D$. The results in Table 9 show that AP-OOD works best on the
 1498 summarization task for both input and output when $M = 512$ and $T = 2$. Although the
 1499 performance drops when decreasing M and increasing T , we find that AP-OOD is relatively
 1500 insensitive to the number of heads and queries.

1501

1502 **Dot product and Euclidean distance.** We compare using the dot product and the
 1503 negative squared Euclidean distance for the attention pooling in AP-OOD. For a formal
 1504 definition of attention pooling with the negative squared Euclidean distance, we refer to
 1505 Appendix D.1. Table 10 shows that using the dot product works substantially better. This
 1506 result aligns with the well-established observation that measuring similarity using the dot
 1507 product in high-dimensional spaces is more effective than using Euclidean distance.

1508

1509

1510 We analyze the inference time of AP-OOD in comparison to the transformer backbone
 1511 and other OOD detection methods. To avoid bottlenecks during data loading, we measure
 1512 inference times on single batches and report the mean and standard deviation across 10

1512

1513 Table 8: Unsupervised OOD detection performance on text summarization. We compare
 1514 results from AP-OOD trained on XSUM as the ID data set when varying β . \downarrow indicates
 1515 “lower is better” and \uparrow “higher is better”. All values in %. We estimate standard deviations
 1516 across five independent dataset splits and training runs.

1517

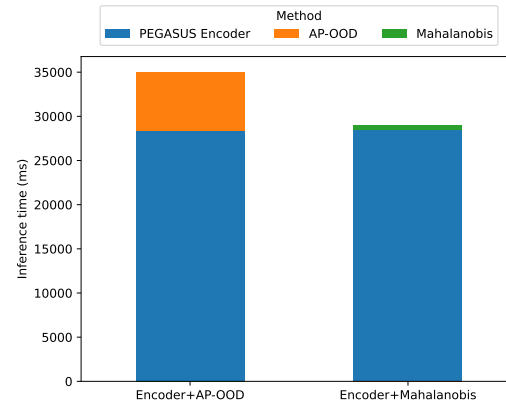
1518

		CNN/DM	Newsroom	Reddit	Samsum	Mean
Input OOD						
$\beta = 0$	AUROC \uparrow	66.83 \pm 0.44	81.42 \pm 0.27	94.81 \pm 0.32	93.38 \pm 0.20	84.11
	FPR95 \downarrow	97.17 \pm 0.10	76.31 \pm 0.35	41.12 \pm 3.42	19.96 \pm 0.84	58.64
$\beta = 0.25$	AUROC \uparrow	97.76\pm0.11	98.75 \pm 0.07	99.87\pm0.06	99.46 \pm 0.09	98.96
	FPR95 \downarrow	11.07\pm0.74	4.75\pm0.41	0.00\pm0.00	0.02\pm0.02	3.96
$\beta = 0.5$	AUROC \uparrow	96.13 \pm 0.44	99.10\pm0.08	99.91\pm0.03	99.80 \pm 0.04	98.74
	FPR95 \downarrow	19.51 \pm 2.24	4.11\pm0.28	0.00\pm0.01	0.04 \pm 0.03	5.91
$\beta = 1$	AUROC \uparrow	91.36 \pm 0.41	98.77 \pm 0.05	99.75 \pm 0.02	99.83 \pm 0.01	97.43
	FPR95 \downarrow	38.78 \pm 4.50	4.94 \pm 0.23	0.02 \pm 0.02	0.00\pm0.00	10.94
$\beta = 2$	AUROC \uparrow	84.29 \pm 0.91	97.58 \pm 0.09	99.52 \pm 0.05	99.76 \pm 0.01	95.28
	FPR95 \downarrow	63.31 \pm 4.63	9.14 \pm 0.46	0.12 \pm 0.07	0.05 \pm 0.03	18.16
$\beta = 1/\sqrt{D}$	AUROC \uparrow	89.09 \pm 0.66	90.59 \pm 0.35	99.59 \pm 0.18	99.87\pm0.01	94.79
	FPR95 \downarrow	53.96 \pm 3.30	47.50 \pm 1.83	0.17 \pm 0.18	0.04 \pm 0.02	25.42
Output OOD						
$\beta = 0$	AUROC \uparrow	77.67 \pm 1.37	85.10 \pm 0.61	84.12 \pm 1.08	91.70 \pm 0.44	84.65
	FPR95 \downarrow	82.07 \pm 1.30	69.32 \pm 1.65	57.30 \pm 1.73	29.37 \pm 1.73	59.52
$\beta = 0.25$	AUROC \uparrow	91.37 \pm 0.64	93.66\pm0.13	94.79 \pm 0.29	96.56 \pm 0.27	94.10
	FPR95 \downarrow	43.03 \pm 1.71	34.70 \pm 0.32	38.38 \pm 3.27	18.61 \pm 2.44	33.68
$\beta = 0.5$	AUROC \uparrow	93.37\pm0.54	92.62 \pm 0.67	98.04\pm0.28	98.30\pm0.11	95.59
	FPR95 \downarrow	23.12\pm1.97	29.91\pm2.93	6.34\pm1.56	6.83\pm0.64	16.55
$\beta = 1$	AUROC \uparrow	93.06 \pm 0.57	91.82 \pm 0.71	97.66\pm0.33	97.91 \pm 0.22	95.11
	FPR95 \downarrow	24.04 \pm 1.95	32.04 \pm 2.97	9.29\pm1.71	8.82 \pm 1.42	18.55
$\beta = 2$	AUROC \uparrow	93.25\pm0.48	91.98 \pm 0.73	97.57 \pm 0.40	97.97\pm0.19	95.19
	FPR95 \downarrow	23.69\pm1.94	31.23\pm3.09	10.06 \pm 2.44	8.37\pm1.30	18.34
$\beta = 1/\sqrt{D}$	AUROC \uparrow	54.67 \pm 0.72	80.59 \pm 0.72	94.12 \pm 0.30	94.93 \pm 0.35	81.08
	FPR95 \downarrow	92.40 \pm 0.21	65.83 \pm 1.03	30.04 \pm 1.15	27.20 \pm 1.94	53.87

1538

1539

1540



1541

1542

1543

1544

1545

1546

1547

1548

1549

1550

1551

1552

1553

Figure 7: Comparing AP-OOD and the Mahalanobis method relative to the encoder inference time. The bars show the mean over ten batches.

1555

1556

1557

1558

1559

1560

1561

1562

1563

1564

1565

batches. Our measurements only start after a warm-up phase of 5 batches. If not stated otherwise, the measurements were performed with a batch size of 32 and context length of 512 tokens. All measurements were performed on a single NVIDIA A100-40GB GPU.

Figure 8 compares the inference time of various OOD detection methods for different batch sizes. As expected AP-OOD has a strong linear relation to the batch size and is significantly slower than the reference models.

Although AP-OOD is slower than other methods like the Mahalanobis method, Figure 7 illustrates that it still takes less than 20 % of the combined inference time of the PEGASUS encoder and OOD detection method. We argue that the higher OOD detection rate mitigates the addition of overhead of AP-OOD since it allows skipping the substantially longer

1566

1567 Table 9: Unsupervised OOD detection performance on text summarization. We compare
 1568 results from AP-OOD trained on XSUM as the ID data set when varying M and T . \downarrow
 1569 indicates “lower is better” and \uparrow “higher is better”. All values in %. We estimate standard
 1570 deviations across five independent dataset splits and training runs.

1571

1572

			CNN/DM	Newsroom	Reddit	Samsum	Mean	
		Input OOD						
1574	$M = 1024$	$T = 1$	AUROC \uparrow	97.16 \pm 0.22	98.25 \pm 0.11	99.82 \pm 0.01	99.32 \pm 0.03	98.64
1575			FPR95 \downarrow	14.72 \pm 0.83	7.54 \pm 0.62	0.00\pm0.00	0.64 \pm 0.11	5.72
1576	$M = 512$	$T = 2$	AUROC \uparrow	97.98\pm0.16	98.83\pm0.07	99.87 \pm 0.03	99.60\pm0.04	99.07
1577			FPR95 \downarrow	9.77\pm0.80	4.67 \pm 0.30	0.00\pm0.00	0.02\pm0.02	3.61
1578	$M = 256$	$T = 4$	AUROC \uparrow	97.76 \pm 0.11	98.75 \pm 0.07	99.87\pm0.06	99.46 \pm 0.09	98.96
1579			FPR95 \downarrow	11.07 \pm 0.74	4.75 \pm 0.41	0.00\pm0.00	0.02 \pm 0.02	3.96
1580	$M = 128$	$T = 8$	AUROC \uparrow	97.53 \pm 0.15	98.49 \pm 0.15	99.83 \pm 0.07	99.14 \pm 0.12	98.75
1581			FPR95 \downarrow	12.48 \pm 1.14	5.94 \pm 0.65	0.00\pm0.00	0.25 \pm 0.10	4.67
1582	$M = 64$	$T = 16$	AUROC \uparrow	97.10 \pm 0.09	98.14 \pm 0.16	99.84 \pm 0.07	98.81 \pm 0.16	98.47
1583			FPR95 \downarrow	14.30 \pm 0.77	7.87 \pm 0.86	0.00 \pm 0.00	0.99 \pm 0.50	5.79
1584	$M = 32$	$T = 32$	AUROC \uparrow	96.84 \pm 0.35	97.78 \pm 0.15	99.83 \pm 0.05	98.56 \pm 0.28	98.25
1585			FPR95 \downarrow	14.97 \pm 1.96	10.18 \pm 0.80	0.01 \pm 0.02	2.53 \pm 2.12	6.92
1586	$M = 16$	$T = 64$	AUROC \uparrow	96.23 \pm 0.45	97.35 \pm 0.24	99.73 \pm 0.11	98.12 \pm 0.24	97.86
1587			FPR95 \downarrow	16.65 \pm 1.99	12.55 \pm 1.15	0.09 \pm 0.20	5.69 \pm 1.87	8.75
1588	$M = 8$	$T = 128$	AUROC \uparrow	95.56 \pm 0.38	96.47 \pm 0.46	99.67 \pm 0.27	97.44 \pm 0.25	97.29
1589			FPR95 \downarrow	18.16 \pm 1.57	16.34 \pm 1.91	0.52 \pm 1.13	11.29 \pm 1.78	11.58
1590	$M = 4$	$T = 256$	AUROC \uparrow	94.58 \pm 0.67	94.75 \pm 0.52	99.27 \pm 0.86	95.24 \pm 0.25	95.96
1591			FPR95 \downarrow	20.10 \pm 2.32	21.71 \pm 2.30	2.01 \pm 4.09	24.58 \pm 1.83	17.10
1592	$M = 2$	$T = 512$	AUROC \uparrow	93.17 \pm 0.75	91.87 \pm 0.56	98.43 \pm 2.39	89.87 \pm 0.86	93.34
1593			FPR95 \downarrow	22.86 \pm 2.20	27.09 \pm 1.48	4.95 \pm 9.38	39.75 \pm 3.06	23.66
1594	$M = 1$	$T = 1024$	AUROC \uparrow	90.90 \pm 1.20	88.10 \pm 0.83	96.68 \pm 5.76	81.41 \pm 1.06	89.27
1595			FPR95 \downarrow	27.14 \pm 3.03	32.64 \pm 2.29	9.03 \pm 16.78	52.73 \pm 3.76	30.39
		Output OOD						
1596	$M = 1024$	$T = 1$	AUROC \uparrow	92.47 \pm 0.48	94.17 \pm 0.30	98.36 \pm 0.22	97.77 \pm 0.14	95.69
1597			FPR95 \downarrow	39.11 \pm 1.81	34.69 \pm 0.85	3.11 \pm 1.16	12.59 \pm 0.90	22.38
1598	$M = 512$	$T = 2$	AUROC \uparrow	93.79\pm0.25	95.85\pm0.18	99.02 \pm 0.20	98.96 \pm 0.06	96.90
1599			FPR95 \downarrow	32.45\pm1.29	20.10\pm0.67	0.95 \pm 0.66	2.77 \pm 0.54	14.07
1600	$M = 256$	$T = 4$	AUROC \uparrow	93.35 \pm 0.46	95.48 \pm 0.28	99.19 \pm 0.26	99.05\pm0.06	96.77
1601			FPR95 \downarrow	33.67 \pm 2.77	21.73 \pm 0.82	0.86\pm0.95	2.72\pm0.52	14.75
1602	$M = 128$	$T = 8$	AUROC \uparrow	93.24 \pm 0.34	95.27 \pm 0.37	99.21\pm0.41	98.99 \pm 0.04	96.68
1603			FPR95 \downarrow	32.84 \pm 1.75	23.40 \pm 1.53	0.99 \pm 1.56	3.26 \pm 0.42	15.12
1604	$M = 64$	$T = 16$	AUROC \uparrow	92.95 \pm 0.82	94.92 \pm 0.39	99.11 \pm 0.36	98.89 \pm 0.14	96.47
1605			FPR95 \downarrow	34.08 \pm 4.22	25.53 \pm 1.87	1.48 \pm 1.63	4.10 \pm 0.70	16.30
1606	$M = 32$	$T = 32$	AUROC \uparrow	92.54 \pm 0.61	94.11 \pm 0.47	98.67 \pm 0.73	98.63 \pm 0.41	95.99
1607			FPR95 \downarrow	37.21 \pm 3.76	29.56 \pm 2.71	4.68 \pm 4.39	6.11 \pm 2.55	19.39
1608	$M = 16$	$T = 64$	AUROC \uparrow	91.26 \pm 1.17	92.62 \pm 1.40	97.99 \pm 2.33	98.58 \pm 0.84	95.11
1609			FPR95 \downarrow	41.96 \pm 4.43	35.78 \pm 5.78	8.75 \pm 13.44	6.19 \pm 4.88	23.17
1610	$M = 8$	$T = 128$	AUROC \uparrow	90.94 \pm 1.97	91.99 \pm 1.88	97.10 \pm 2.54	98.28 \pm 0.80	94.58
1611			FPR95 \downarrow	41.24 \pm 8.00	36.42 \pm 7.58	13.13 \pm 13.35	7.58 \pm 3.85	24.59
1612	$M = 4$	$T = 256$	AUROC \uparrow	89.62 \pm 1.80	90.35 \pm 2.64	95.91 \pm 3.26	97.73 \pm 0.96	93.40
1613			FPR95 \downarrow	47.52 \pm 9.04	41.77 \pm 12.21	18.53 \pm 16.24	10.02 \pm 4.76	29.46
1614	$M = 2$	$T = 512$	AUROC \uparrow	87.82 \pm 2.50	88.06 \pm 1.29	94.00 \pm 3.38	96.91 \pm 1.26	91.70
1615			FPR95 \downarrow	52.18 \pm 9.71	50.66 \pm 5.51	28.44 \pm 17.40	13.98 \pm 6.18	36.31
1616	$M = 1$	$T = 1024$	AUROC \uparrow	86.45 \pm 1.86	86.95 \pm 1.79	93.43 \pm 2.35	96.10 \pm 1.59	90.73
1617			FPR95 \downarrow	50.92 \pm 8.94	49.61 \pm 6.70	29.61 \pm 8.37	14.82 \pm 3.62	36.24

generation time more often (see Table 11). The degree to which the overhead of AP-OOD is mitigated by skipping the decoder depends on the rate of detected OOD samples in future applications.

The heatmap in Figure 9 shows the inference time of AP-OOD for different selections of the hyperparameter number of heads M and number of queries T . While for small values of both parameters the inference time is constant, for larger parameters the inference time increases linearly with both parameters.

The inference time of the decoder of the transformer depends on the length of the longest output sequence of a batch. To obtain consistent measurements, we forced the decoder to always produce the same sequence length. Figure 10 illustrates the inference times of the PEGASUS transformer model. The plots of the first row cover the performance of the PEGASUS encoder only, while the second row shows the combined inference time of the encoder and decoder. In the left column, the plots indicate that the model inference time increases linearly with the batch size. Further, it is shown that the encoder takes about 10 % of the overall inference time. The right column shows the inference times for

1620

1621 Table 10: Unsupervised OOD detection performance on text summarization. We compare
 1622 results from AP-OOD trained on XSUM as the ID data set when using the dot product and
 1623 the Euclidean similarity. \downarrow indicates “lower is better” and \uparrow “higher is better”. All values in
 1624 %. We estimate standard deviations across five independent dataset splits and training runs.

1625

1626

		CNN/DM	Newsroom	Reddit	Samsum	Mean
Input OOD						
Dot product	AUROC \uparrow	97.76\pm0.11	98.75\pm0.07	99.87\pm0.06	99.46\pm0.09	98.96
	FPR95 \downarrow	11.07\pm0.74	4.75\pm0.41	0.00\pm0.00	0.02\pm0.02	3.96
Euclidean	AUROC \uparrow	74.22 \pm 0.65	84.43 \pm 0.23	97.06 \pm 0.41	98.30 \pm 0.23	88.50
	FPR95 \downarrow	90.20 \pm 0.37	74.08 \pm 1.04	15.27 \pm 5.30	7.17 \pm 1.94	46.68
Output OOD						
Dot product	AUROC \uparrow	93.37\pm0.54	92.62\pm0.65	98.04\pm0.29	98.30\pm0.11	95.58
	FPR95 \downarrow	23.12\pm1.98	29.93\pm2.89	6.36\pm1.60	6.83\pm0.64	16.56
Euclidean	AUROC \uparrow	87.67 \pm 0.74	88.17 \pm 1.80	96.50 \pm 0.57	91.28 \pm 1.79	90.90
	FPR95 \downarrow	65.69 \pm 3.90	66.04 \pm 4.38	22.34 \pm 5.36	53.89 \pm 7.80	51.97

1635

1636 Table 11: Inference times of OOD methods and PEGASUS transformer for a batch size
 1637 of 32 samples, number of heads $M = 256$, number of queries $T = 4$, and a context length
 1638 of $S = 512$ tokens. All values in milliseconds ms . We estimate the mean and standard
 1639 deviation over ten batches.

1640

AP-OOD	Mahalanobis	PEGASUS Encoder	PEGASUS Generation
6.58 \pm 0.095	0.52 \pm 0.146	28.43 \pm 2.513	34940.34 \pm 65.842

1642

1643

1644 an increasing number of context tokens. The inference time of the transformer encoder and
 1645 decoder increases quadratically with the context length.

1646

1647

E THE USE OF LARGE LANGUAGE MODELS

1648

1649

1650 When creating this paper, we utilized large language models (LLMs) to refine our writing,
 1651 to identify related work, and for research ideation. When refining the writing using LLMs,
 1652 we carefully review and verify LLM output to preserve sentence semantics. For related work,
 1653 we confirm the soundness of papers suggested by the LLM, and for research ideation, we
 1654 verify the factual accuracy of all statements.

1655

1656

1657

1658

1659

1660

1661

1662

1663

1664

1665

1666

1667

1668

1669

1670

1671

1672

1673

1674

1675

1676

1677

1678

1679

1680

1681

1682

1683

1684

1685

1686

1687

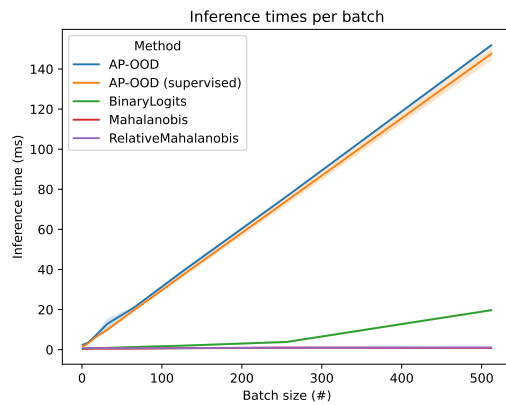
1688

1689 Figure 8: Comparison of various OOD detection methods for increasing batch sizes. We
1690 estimate the mean and standard deviation over ten batches.

1691

1692

1693



1694

1695

1696

1697

1698

1699

1700

1701

1702

1703

1704

1705

1706

1707 Figure 9: Inference times for AP-OOD over different numbers of heads M and queries T .
1708 We estimate the mean over ten batches.

1709

1710

1711

1712

1713

1714

1715

1716

1717

1718

1719

1720

1721

1722

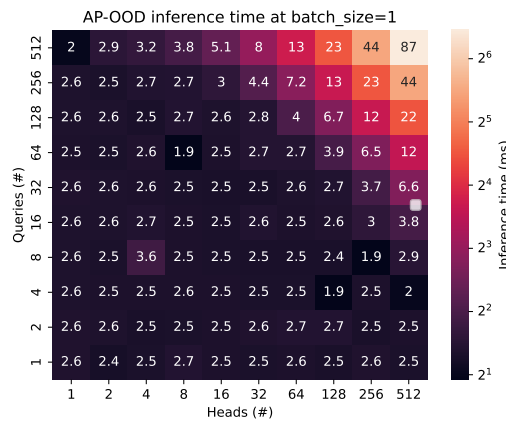
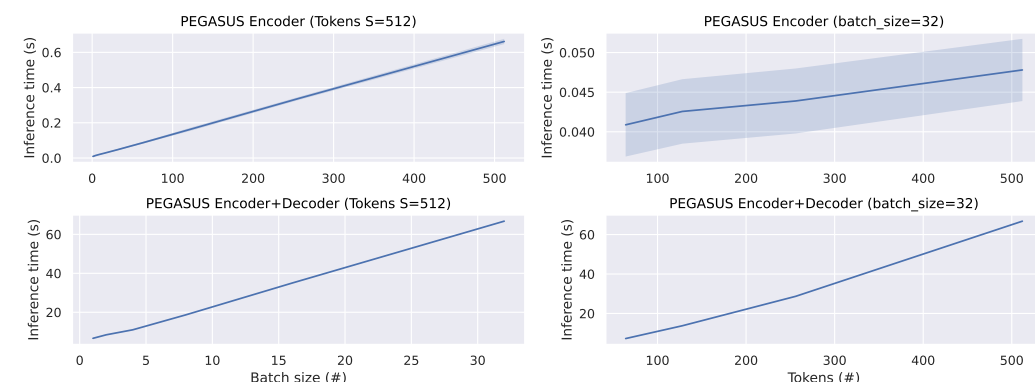
1723

1724

1725

1726

1727

1728 Figure 10: Inference times for the PEGASUS model for various batch sizes (left) and various
1729 numbers of input tokens (right). The top row illustrates the Encoder's performance, while
1730 the bottom row shows the combined performance of the Encoder and Decoder. We estimate
1731 the mean and standard deviation over ten batches.1732 Figure 10: Inference times for the PEGASUS model for various batch sizes (left) and various
1733 numbers of input tokens (right). The top row illustrates the Encoder's performance, while
1734 the bottom row shows the combined performance of the Encoder and Decoder. We estimate
1735 the mean and standard deviation over ten batches.